UNIVERSITY OF TARTU

FACULTY OF SCIENCE AND TECHNOLOGY

Institute of Chemistry

Master's Thesis (30 EAP)

Applied Measurement Science

Zeinab Chehreghan

UNCERTAINTY OF THE OPTICAL SPECTRAL TRANSMITTANCE

Supervisor: Ilmar Ansko

Tartu 2023

MASTER'S THESIS	
University of Tartu	
Faculty of Science and Technology	
Institute of Chemistry	
Degree Programme:	Applied Measurement Science
Author:	Zeinab Chehreghan
Title:	Uncertainty of the optical spectral transmittance Optilise spektraalse läbilaskvuse mõõtemääramatus
Supervisor (Tartu Observatory):	Ilmar Ansko

Abstract: Determination of the optical filter spectral transmittance takes place at Tartu Observatory and is one of the accredited methods of the Tartu University Testing Centre. Comprehensive characterization of the measurement setup forms the experimental part of this master thesis. The measurement principles, instrumentation, and techniques are described in detail. In conclusion, the uncertainty contributions were quantified, and recommendations were given in order to improve the measurement setup. The thesis can be used as step-by-step instructions when reproducing the characterization of similar systems.

Kokkuvõte: Optiliste filtrite spektraalse läbilaskvuse mõõtmine Tartu Observatooriumi optikalaboris kuul-ub Tartu Ülikooli Katsekoja akrediteeritud meetodite hulka. Magistritöö käigus viidi läbi mõõtesüsteemi põhjalik karakteriseerimine. Detailselt on kirjeldatud mõõtmise aluspõhimõtted, aparatuur ja mõõtemeetodid. Töö tulemusena täpsustati määramatuse kom-ponente ja anti soovitused meetodi täiustamiseks. Magistritöö on kasutatav käsiraamatuna sarnaste süsteemide karakteriseeriminsel.

Keywords:	optical transmittance, characterization, uncertainty
Märksõnad:	optiline läbilaskvus, karakteriseerimine, mõõtemääramatus
CERCS code:	P180
Number of pages:	62
Language:	English
Date:	23.05.2023

Contents

Abbreviations

ADC	Analog to Digital Converter
BW	Bandwidth
CWL	Central Wavelength
DC	Direct Current
FOV	Field of View
FWHM	Full Width at Half Maximum
GOF	Goodness Of Fit
N/A	Not Applicable
NIR	Near Infrared
PID	Proportional Integral Derivative
PMT	Photomultiplier Tube
PSU	Power Supply Unit
RMS	Root Mean Square
SLF	Slit scattering function
SN	Serial Number
SNR	Signal-to-Noise Ratio
UV	Ultraviolet
WAS	Wasabi prototype radiometer
WL	Wavelength

1. INTRODUCTION

The aim of the current thesis is to review and update the uncertainty budget of the optical filter transmittance by re-characterizing the key components of the measurement setup. Determination of the filter transmittance takes place in Tartu Observatory and is one of the accredited methods (M807) under the umbrella of the Tartu University Testing Centre. Moreover, three more accredited methods depend on the filter transmittance: spectral irradiance (M804) and radiance (M805) responsivity and incandescent lamp calibration (M806). The spectral transmittance method was updated during this work, and recommendations were given for further improvements. This thesis is also meant as a characterization guide for method M807, as the literature covering necessary equipment and measurement techniques is sparse otherwise.

2. MOTIVATION

2.1. The spectral transmittance

Transmittance is a dimensionless number defined by the ratio of the radiant flux transmitted (Φ_t) to the incident radiant flux (Φ_i). Conservation of energy dictates that the transmittance for nonfluorescent materials have values in the interval 0–1. [1]

$$\tau(\lambda) = \frac{\Phi_t(\lambda)}{\Phi_i(\lambda)}$$

Spectral transmittance is defined by the ratio of the transmitted power *I(λ)* to the incident power I_0 *(λ)* in a small wavelength interval around the center wavelength *λ*. [2]

$$\tau(\lambda) = \frac{I(\lambda)}{I_0(\lambda)}$$

Determination of the spectral transmittance is essential when investigating the material properties and as a side characterization in a vast number of experimental methods in physics, chemistry, biology/medicine, applied sciences, and technology. The transmittance of gaseous, liquid, or solid substances can be measured. The principle is shown in Figure 2-1. When the parallel light beam is incident on the matter, the radiation will be partially reflected from the boundaries, partially absorbed or scattered by the bulk material, and partially transmitted.

In optical physics, the intensity *I* is generally understood to be the optical power per unit area, which is transmitted through an imagined surface perpendicular to the propagation direction. For a monochromatic propagating wave, the local intensity is related to the amplitude of the electric field via $I \propto |E|^2$ [3]. As stated by the energy conservation law, the power of the incident beam should be equal to the total power of reflected, absorbed, scattered, and transmitted beams:

$$I = I_r + I_a + I_s + I_t$$

(I is the intensity of the incident beam, I_r is the intensity of the reflected beam, I_a is the intensity of the absorbed beam, I_s is the intensity of the scattered beam, and I_t is the intensity of the transmitted beam.)

Figure 2-1 Filter transmittance.

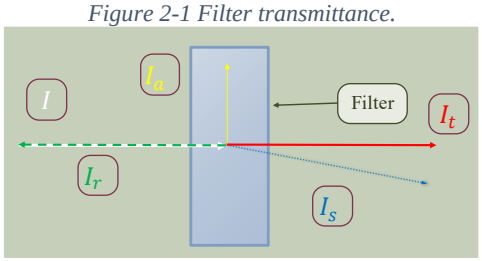

2.2. Spectrophotometer

The apparatus for transmittance determination is historically called “spectrophotometer", although the applicable wavelength range usually exceeds the visible portion of the electromagnetic spectrum. The typical construction of a stand-alone spectrophotometer is shown in Figure 2-2.

The apparatus consists of one or more broadband light sources in order to cover the needed wavelength range with a high enough signal-to-noise ratio (SNR), a monochromator, a sample holder, and a detector. At the exit slit of the monochromator, a quasi-parallel light beam is often formed with additional optics, or a monochromator with a long focal length is used. Construction of the sample compartment depends on the properties of the filter. Sometimes, the spectrophotometer supports sample holders for various filter phases (solid, liquid, gaseous).

Figure 2-2 The spectrophotometer. 1) light source; 2) monochromator; 3) collimating optics; 4) sample holder; 5) detector.

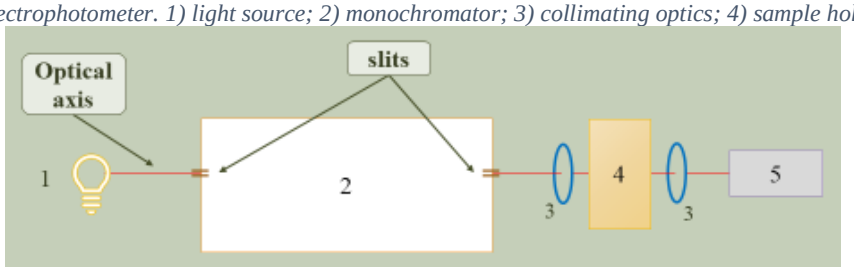

The measurement process consists of scanning the incident radiation wavelength-by-wavelength over the range of interest and registering the intensity of the transmitted radiation. The bandwidth of the incident light is relevant when investigating the narrow spectral effects. In order to derive the transmittance of the filter under test, the transmitted intensity has to be normalized (i.e., divided) by the reference signal, which is usually recorded in the same regime without the filter. The beam geometry for the filter and reference should be precisely the same. The so-called dual-beam spectrophotometers have two identical multiplexed optical paths, and the reference signal can be retrieved quasi-simultaneously with the filter measurement. The transmittance can be corrected with a particular reference signal selection, e.g., the boundary reflections. Depending on the detector system, separated dark scans might be needed.

Depending on the object parameters and measurement task, the spectrophotometer can be modified or simplified, for example, Acoustic resonance spectroscopy [4], Fluorescence spectroscopy [5], One-drop spectroscopy [6] by Filter photometer [7], or diode array spectrophotometer [8].

2.3. Limitations and Uncertainties

The precision of the filter transmittance result is determined by many factors, which can be divided into three groups: etalon-related, method-related, and object-related.

As the transmittance measurement is inherently the ratio of two signals, uncertainty and drift of the light sources will not affect the result directly. Exceptions are the possible short-term instability or flickering. Monochromator's wavelength scale and bandwidth act as the primary source of etalon-related uncertainty. The wavelength scale might have bias, random error, hysteresis, and temperature- and time-dependent drift [9]. The monochromator also determines spectral purity and spatial uniformity of the radiation field at the filter.

The method-related uncertainty components include repeatability of the filter placement, diffraction of the light beam, environmental effects, etc. By careful measurement plan, many of the uncertainty components can be significantly reduced or quantified and compensated for.

The object-related uncertainty contains, e.g., the spatial and temporal non-uniformity of the filter and the temperature and angular dependency of the transmittance. It is up to the task definition how these properties can be handled in order to characterize the object so that the results can be applied for later usage. For the best results, the characterization conditions should match the field usage as closely as possible.

2.4. METHOD M807:28.02.2022, Calibration of filter transmittance

Method M807 uses a slightly modified measurement principle compared to Figure 2-2. The stand-alone spectrophotometer is replaced by a double grating monochromator in order to reduce the spectral stray light significantly and allow flexible usage of light sources, filter holders, and detectors. A Ø3 mm aperture constrains the light beam. Considering the small aperture and ~ 0.5 mm slit width, the beam's divergence is only about 2 °, and collimating optics is unnecessary. However, the beam's intensity and spectral constitution have to be measured. A ribbon filament lamp is used as the light source, providing excellent spatial uniformity of the light beam. This allows one to use a short focal length monochromator, increasing the optical throughput of the system. The M807 setup is suitable for a comprehensive characterization of

the system components. Finally, the method is periodically validated via inter-comparison measurements.

In order to support the transition to the new monochromator model, the existing one was carefully characterized during this master thesis. The characterization techniques and results will be described in the following chapters. Also, the method's limitations are pointed out, and possible ways of improvement are suggested. As one result of the thesis, the M807 method document will be updated.

In the context of method M807, a filter radiometer consisting of a precision aperture, temperature-controlled interference filters, and a 3-diode reflection trap detector is used (see 3.1). The filter radiometer acts as a stand-alone etalon detector for spectral irradiance. Method M807 is particularly important because it supports three additional accredited calibration methods. The filter radiometer acts as an independent lamp intensity monitor for the spectral irradiance and radiance calibration methods M804 and M805. In the incandescent lamp calibration method M806, the filter radiometer is used as a transfer radiometer. The filter radiometer will be described in 3.1.4.

3. METHODS AND INSTRUMENTS

3.1. The measurement setup

The M807 filter spectral transmittance measurement setup is shown in Figure 3-1. This setup is referred to as the "standard measurement setup" in this document because primarily used in the framework of M807. The double monochromator, trap detector with filter holder, ribbon filament lamp (RFL), and condenser lens are used. Not shown in Figure 3-1 are the power supplies, monitoring and recording devices, and controlling computer. The condenser lens makes the incident lights focused on the entrance slit. The double monochromator selects under the computer control portion of the spectrum with certain CWL and bandwidth. The light enters the radiometer via a precision aperture, passes the filter, and is converted into electric current by the 3-element silicon trap detector. The filter radiometer is attached to the monochromator with a special adapter, allowing fast and repeatable alignment. The output signal is converted into digital numbers and stored for further analysis. The scanning parameters (spectral range, step, bandwidth, integration time) are set by the user.

Figure 3-1 The measurement setup [10]

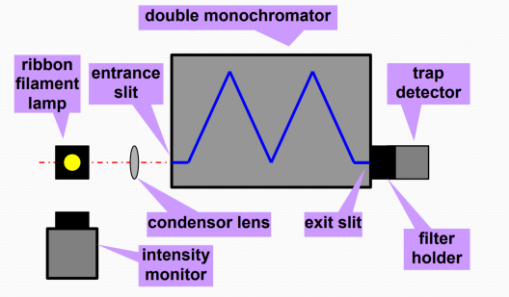

As the filter properties dictate, the light source and detector compartments can be modified. A detailed description of the setup components is given in the following subchapters. The next chapter will describe additional hardware used in this work.

Air temperature, relative humidity, and atmospheric pressure in the laboratory are constantly monitored by a dedicated logger. The electrical, optical, and environmental parameters are automatically recorded in a computer database and can be monitored via a web interface.

The environmental conditions for the cleanrooms and laboratories are outlined as follows: The cleanrooms maintain ISO 8 (100,000) class air quality, with an overpressure of (10-15) Pa between the entrance and subsequent cleanrooms. The laboratories are controlled at a temperature

of (22 ± 3) °C, while the relative humidity in the rooms is maintained at (55 ± 10)%. The laboratory adheres to ISO/IEC 17025:2006 and ECSS-Q-ST-70-01C[1].

3.1.1. Double monochromator

The monochromator is a Bentham Instruments Ltd. DTMS300. The optical scheme is shown in Figure 3-2, and the key parameters are listed in Table 3-1. This high-performance, triple-grating, double monochromator was designed for applications requiring superior scattered light performance. It consists of two single-monochromators arranged in an additive configuration, offering exceptional optical performance and flexibility in configuration. This provides the advantage of internal motorized slits for easy maintenance and adjustable measurement bandwidth. It supports up to three diffraction gratings per monochromator and offers multiple entrance and exit ports with automated mirror-based port selection for diverse input/output/detector configurations [11]. (Read more in Table 9-1)

Figure 3-2 The schematic of the triple grating double monochromator

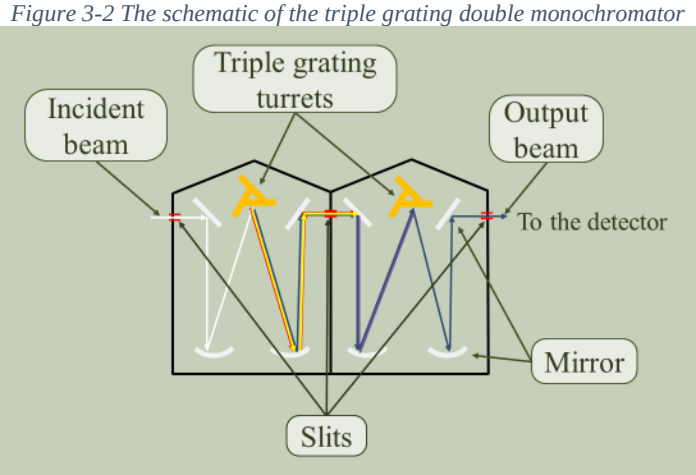

Table 3-1 Parameters of the monochromator

Parameter	Value	unit
optical design	Double Czerny-Turner dispersions added	N/A
focal length	300	mm
F-number	1/4.1	-
Grating size	68x84	mm
interface	USB 2.0	-
wavelength range	200-2500	nm
Filter size (diameter)	23	mm

[1] Laboratory environmental conditions PROCEDURE PR805:23.08.2018 by TESTING CENTRE OF UNIVERSITY OF TARTU

3.1.2. The ribbon filament lamp

The ribbon filament lamp is mainly used in the standard setup because it provides the most uniform light field for the transmittance measurement. The lamp is a Soviet SI300/10 bulb mounted in the stand allowing precise alignment, and equipped with the power supply, which was produced at Tartu Observatory, based on the modified computer PSU in constant current mode and external precision one milli-ohm shunt resistor type P310 (see Table 9-5). The lamp current is 30.000 A at approx. 10 VDC. Drift and ripple are below 0.1 mA. The lamp and power supply are shown in Figure 3-3. Dimensions of the working area of the RFL are 17 mm x 3.2 mm. (Read more in Table 9-3 and Table 9-4)

Figure 3-3 The ribbon filament lamp.

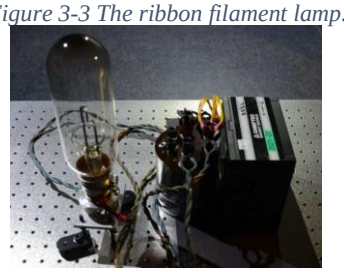

3.1.3. The collimating lens.

The RFL is focused on the monochromator's entrance slit by a Ø60 mm quartz lens.

3.1.4. The filter radiometer

The filter radiometer has a triple function. It acts as 1) a filter holder for the D0.5" (12.5 mm) and D1" (25 mm) circular filters (including thermal control), 2) a precision D3 mm aperture in front of the filter, and 3) a light detector. Construction and the external look of the radiometer are shown in Figure 3-4. The Peltier cooler is essential for narrow-band interference filters, as their transmittance depends on temperature. The reflectance type trap detector [12], based on three windowless Si diodes Hamamatsu S1337BQ-1010 [13], is designed for absolute spectral irradiance needs but acts merely as a light detector here. The filter radiometer is placed at the exit slit of the monochromator via a specially designed adapter. The adapter allows quick and precise installation of the radiometer with high repeatability needed during the filter and reference measurements. The filters with prefabricated holders are installed manually. For the reference measurement, an empty filter holder is installed. (Read more in Table 9-12)

Figure 3-4 a) Schematic layout of the designed filter radiometer. The figures denote 1) brass mounting ring, 2) aperture holder with precision aperture, 3) metallic enclosure with filter, 4) metallic heater/cooler incl copper heater, plastic isolator, and Peltier' thermocooler, 5) plastic centering ring, 6) 3-Si diode trap detector, 7) electrical connector; b) Photo of the assembled filter-radiometer [14] c) installed on the monochromator.

3.1.5. Control and electronics

The trap detector signal is digitalized using a Bentham 487 preamplifier with ADC. The monochromator and 487 are connected to the PC-type computer and controlled by specialized software. The software allows one to set the scanning parameters, measure the spectra, control the monochromator's shutter, monitor the connected devices' health, etc. The scan results are stored in the disk files for further processing. (see Figure 9-6)

3.1.6. Temperature controller

The Newport Corporation 350B [15] is a temperature controller used to maintain precise temperature control of the filter. It utilizes a proportional-integral-derivative (PID) control algorithm to adjust the current of the Peltier' element, which controls the temperature of the filter holder. The 350B has a temperature control down to ±0.005 °C and can operate in heating and cooling modes. Temperature control is critical when measuring the transmittance of the interference filters. (Read more in Table 9-9)

3.2. Characterization equipment

During the characterization measurements described in this thesis, additional instruments were used, not needed in the M807 standard setup. These devices will be shortly described in the following subchapters and referenced later in the corresponding measurement chapters.

3.2.1. The Kr and Hg pen ray lamps

Kr and Hg are "pen ray" gas-discharge lamps (Figure 3-5) from L.O.T. Oriel LSPxxx commonly used as light sources for spectroscopy [16]. They emit a range of distinct, narrow-band spectral lines that can be used for wavelength calibration in various applications. The dimensions of the radiating volume are 3 mm x 50 mm. Hg has intensive lines primarily in the ultraviolet region, while Kr emits lines across a broad range of visible and ultraviolet regions. During the characterization measurements, the lamp is either focused directly on the entrance slit

with a lens or placed close to the entrance aperture of the integrating sphere. The power supply is used in conjunction with the system. (Read more in Table 9-2)

Figure 3-5 The Pen-Ray lamp with power supply.

3.2.2. The Laser Pointer LT52

The Laser Pointer LT52 Figure 3-6 emits a narrow beam of coherent light at a wavelength of 655 nm. It uses a diode laser as the light source and operates on a battery. The LT52 is commonly used for various applications' alignment, positioning, and pointing tasks. The LT52 includes a pinhole aperture which makes it superior compared to the alternatives when precise positioning is crucial. (Read more in Table 9-7)

Figure 3-6 XCL (left) and Alignment lases LT52 (right)

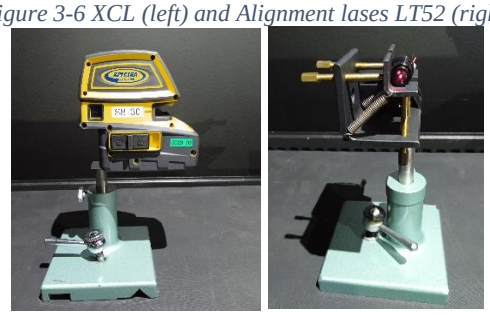

3.2.3. The Laser Pointer XCL

The Laser Pointer XCL is a dual-beam construction laser at ~650 nm. The alignment lasers are shown in Figure 3-6. The dual-beam property is especially advantageous when defining the optical axes of the setup. The divergence between the beams is periodically characterized and documented. (Read more in Table 9-8)

3.2.4. The HeNe laser

The HeNe laser (SN HRS015) is a gas discharge laser that produces a highly coherent beam of light at 633 nm. It consists of a glass tube containing a mixture of helium and neon gas. The HeNe laser is widely used in scientific and technical applications, such as interferometry and alignment. This model is intensity stabilized and is usable in many characterization measurements. The output power of the HeNe laser is superior as well, compared to the solid-state alignment lasers.

3.2.5. *The Bentham integrating sphere.*

The integrating sphere Bentham (DIFF_D8_SLIT_FIBRE) [17] is a hollow, spherical enclosure coated internally with a diffuse white reflective material (Figure 9-1). The sphere ensures that all of the light entering the sphere is reflected multiple times before exiting the output aperture. This makes the light field at the sphere's output spatially uniform. The Bentham integrating sphere is matched with the entrance slit of the monochromator (see 3.3) and allows one to enlighten the monochromator's exit slit in a highly repeatable manner. The sphere is used for wavelength calibration of the monochromator. (Read more in Table 9-6)

3.2.6. *DC AMP/ADC*

DC AMP/ADC [18] is a combination of a DC amplifier and an analog-to-digital converter (ADC) that is used to measure and digitize analog electrical signals. The trans-impedance amplifier converts the small current signal from the detector into DC voltage. The ADC converts the voltage into a digital signal that a computer or other digital devices can process. (Read more in Table 9-11 and Figure 9-3)

3.2.7. *The PhotoMultiplier Tube*

The photomultiplier tube PMT-TO-1 [19] is a photoelectron that converts incident light into electrical current. It consists of a vacuum tube with a photo-emissive surface, a series of dynodes, and an anode. When light strikes the photo-emissive surface, it emits electrons which are then accelerated towards the anode by the dynodes, resulting in a significant multiplication of electrons and a corresponding increase in signal. The photomultiplier tube is used in some characterization measurements because of its superior sensitivity to solid-state detectors. (read more in Figure 9-2 and Table 9-10)

3.2.8. *The Wasatch spectrometer*

The Wasatch WP-VISNIR-R2-IC OEM spectrometer (Figure 9-5) utilizes transmission volume phase grating technology, a Hamamatsu S10420-1106 (14x14) µm pixel back-thinned CCD sensor, and internal TEC cooling. It features an f/2.0 input aperture designed as an SMA-905 fiber adapter. The spectrometer is equipped with acquisition electronics, a thermal controller, and a USB version 2.0 interface *[20]*. Detailed technical specifications can be found in

Table 9-13. The fiber input was equipped with a Ø3 mm aperture during the characterization measurements, mimicking the standard measurement conditions.

3.3. The Alignment

In order to take full advantage of the optomechanical properties of a monochromator, specific geometrical considerations have to be taken into account, and alignment procedures followed. The proper alignment ensures that the CWL and bandwidth are well defined during the measurements, the optical throughput and resolving power correspond to the specification, and there are no unwanted effects such as spectral stray light. The alignment of internal components of the monochromator is expected to be optimal and not covered here. The simplified input optics of the monochromator is shown in Figure 3-7. The monochromator's focal length and input aperture are shown in Table 3-1. The input aperture, the diameter of the lens, or the sphere's exit aperture determine the optimal geometry of the light cone. The rays from the edges of the lens or the aperture shall hit the edges of the collimating mirror and fill the grating (green lines in Figure 3-7). The distance of the lens (aperture) thus depends on the diameter of the lens (aperture). In the case of the lens, the light source is placed so that its sharp image is formed on the entrance slit. If possible, the lens's focal length and the light source's dimensions (the filament or discharge) are chosen to overfill the entrance slit just slightly. This guarantees the best energetic efficiency of the setup. When the input cone underfills the monochromator's numeric aperture, only part of the grating will take part in the diffraction (blue lines in Figure 3-7). As the grating's resolving power is proportional to the total number of grooves

$$R = \frac{\lambda}{\Delta\lambda} = mN \tag{3-1}$$

(R is the grating's resolving power, λ is the central wavelength, $\Delta\lambda$ is the smallest resolvable wavelength difference, m is the order of diffraction, and N is the total number of grooves in the grating that are illuminated by the source [21]), the spectral resolution at the exit slit will be reduced. The total amount of energy passing the monochromator will be reduced as well. If the entrance cone overfills the collimating mirror (red lines in Figure 3-7), part of the light will be scattered inside the monochromator. Not only will this reduce energy efficiency, but it also creates a threat of spectral stray light. In that case, part of the light from the entrance slit passes to the exit slit by random reflections and scattering, the monochromator's apparatus function will be distorted, and the radiometric range will be seriously compromised. Determination of the spectral stray light will be described in 4.5.

Figure 3-7 Illumination of the entrance slit with the lens. 1) lens; 2) entrance slit; 3) collimator; 4) grating; 5) optical axis.

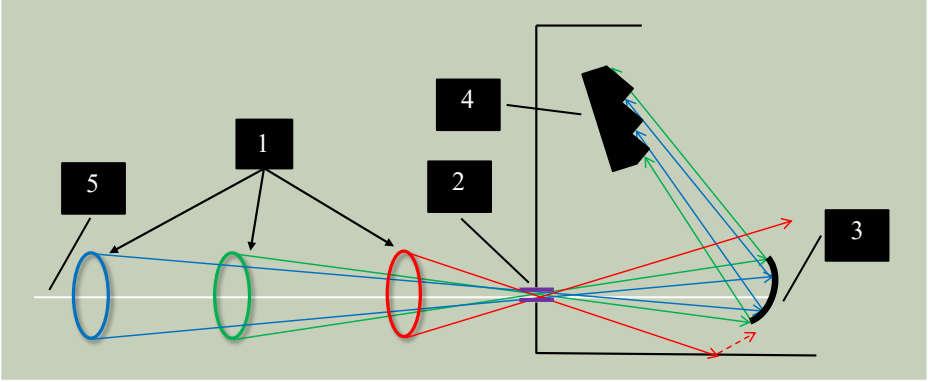

The spectral bandwidth of the exiting radiation depends on the widths of the entrance and exit slits, as the slit widths are generally chosen to be equal [22]. The narrower the slits, the smaller the bandwidth. However, the lower limit of the bandwidth is limited by the diffraction parameters of the gratings and slits and cannot be infinitely small. This limit is called "the slit normal width". When the slits are wider than normal, the spectral resolution will be compromised, but the throughput will increase. When the slits are narrower than normal, the spectral resolution will not improve, but the throughput will. The apparent shapes of output spectra will be analyzed in Chapter 3.4. The normal width will be experimentally determined in chapters 4.2 and 5.2.

3.4. Line Fitting Techniques

Most monochromator-specific characterization measurements result in the scan of intensity (i.e., detector signal) in respect of the wavelength or coordinate. The geometrical shape often presents a single maximum of arbitrary width and shape. To reliably quantify the geometrical shape, a set of statistics is needed. From the practical point of view, the techniques called "line fitting" were used. Line fitting is a needed tool for many scientific applications, especially for spectral measurements, and selections of software products are available. Python libraries (NumPy), Origin, and MATLAB (peakfit and deconvolution) are among the available options for achieving this goal. CWL, FWHM, and peak area are essential parameters for the current work. The line shapes depend on the characterization task (see Figure 3-8 to Figure 3-10), and the representative algorithm has to be chosen for each shape. For the algorithm selection, as well as for the later usage, a consistent fitting parameter should exist.

The fitting of peaks in MATLAB was performed using the 'peakfit'. The code, obtained from the MATLAB website, is a library that offers the capability to fit peaks to 45 different shapes. However, only six shapes were considered necessary for this study, Gaussian, Lorentzian, Voigt profile, Triangular, Flattened Gaussian, and Rectangular, and explained in 3.4.1 to 3.4.4.

The root mean square (RMS) fitting error can be used to select the best fit for your peak analysis. It quantifies the average difference between the fitted model and the observed data points within a specified segment. A lower RMS value indicates a better fit, reflecting a smaller average discrepancy between the model and the observed data. The one that provides the most accurate representation of the observed data within the segment can be identified by comparing the RMS fitting errors of different models. This objective evaluation helps make informed decisions and choose the best-fitting model for the peak analysis. (see 9.1)

In cases where none of the shapes provided a satisfactory fit, an alternative code was utilized to extract the required information directly. The details of this alternative approach will be elaborated upon in 3.4.6.

3.4.1. Triangular

At the normal (and smaller than normal) slit widths (see 3.3), the shape of a well-aligned monochromator is close to triangular.

The "fittriangular" function takes the peak position and width as input parameters and performs the fitting between the observed data and the computed values based on the triangular function. The "triangular" function calculates the shape of the triangular peaks. It takes the position and half-width as input parameters and generates the triangular waveform. Figure 3-8 shows a sample spectrum and fitted peak to a Triangular shape.

The mathematical algorithms related to the triangular shape can be found in 9.1.3.

Figure 3-8 The spectrum and fitted peak to a Triangular shape.

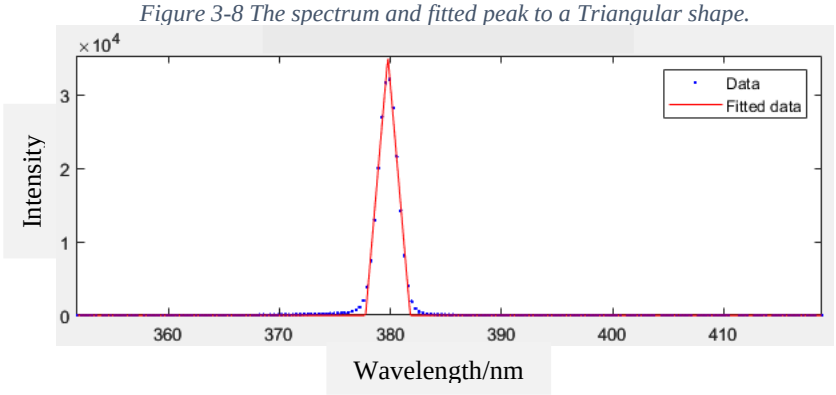

This fitting shape is used to extract peak parameters in Chapters 4.2 and 4.4. Table 9-14 shows the error in percentage for some spectra. It determines that the Triangular peak shape best fits the spectra.

3.4.2. *trapezoidal*

When the slits are wider than normal, the spectral shape tends to be trapezoidal. In this thesis, the trapezoidal case is treated in general terms, as shown in 3.4.6.

3.4.3. *Gaussian, Lorentzian, and Rectangular*

The “fitgaussian” function takes the peak position and width as input parameters and performs the fitting between the observed data and the computed values based on the Gaussian function. The “Gaussian” function calculates the shape of the Gaussian peaks. It takes the position and half-width as input parameters and generates the Gaussian waveform. Figure 3-9 shows a spectrum and the fitted peak to a Gaussian shape.

The mathematical algorithms related to the Gaussian shape can be found in 9.1.1.

This fitting shape is used to extract peak parameters in Chapters 4.2, 4.3, 4.4, 4.5, and 4.8. For example, Table 9-14 shows the error in percentage for some spectra. It determines that the Gaussian peak shape best fits the spectra.

Figure 3-9 The spectrum and fitted peak to a Gaussian shape.

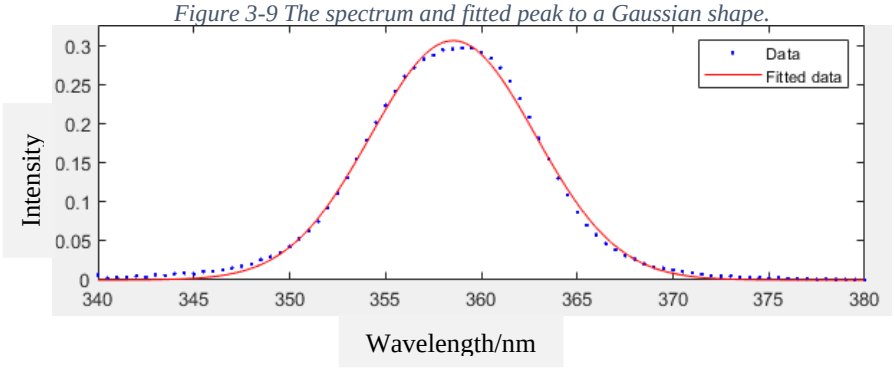

The Lorentzian and Rectangular peak shapes were analyzed using the same procedure. The mathematical algorithms related to the Lorentzian and Rectangular shapes can be found in 9.1.2 and 9.1.4, respectively. It is worth noting that neither the Lorentzian nor the Rectangular shapes provided the best fit in any of the cases.

3.4.4. *Voigt profile and Flattened Gaussian*

The “fitvoigt” function takes the peak position, the Doppler (Gaussian) width, and the shape constant as input parameters. It fits the observed data and the computed values based on the Gaussian function. The “voigt” function calculates the shape of the voigt peaks. The Voigt profile is a convolution of the Gaussian and Lorentzian functions, and its parameters include the position, the Doppler width, and the shape constant. The Voigt profile did not provide the best fit in any of the cases.

The mathematical algorithms related to the Voigt shape can be found in 9.1.5.

The Flattened Gaussian peak shape was analyzed using the same procedure. Figure 3-10 shows a spectrum and the fitted peak to a Flattened Gaussian shape. The mathematical algorithms related to the Flattened Gaussian shape can be found in 9.1.6.

Figure 3-10 The spectrum and fitted peak to a Flattened Gaussian shape.

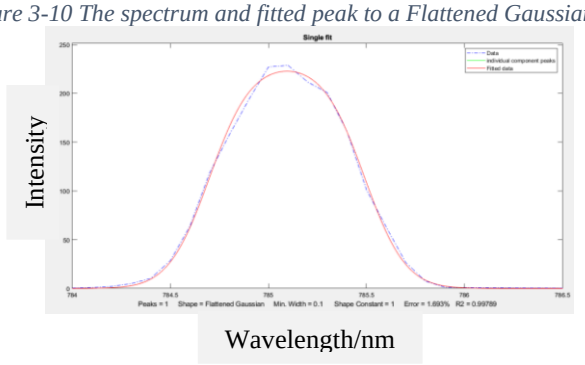

This fitting shape is used to extract peak parameters in Chapters 4.1, 4.2, 4.3, and 4.5. For example, Table 9-16 shows the error in percentage for some spectra. It determines that the Flattened Gaussian peak shape best fits the spectra.

3.4.5. Arbitrary

There are cases when the spectral shape does not conform with any of the previously described, but the numeric characterization is still needed. One example is the narrow-band interference filters used in methods M804-M806 (Figure 3-11). In that case, the quantities are defined which are most useful for the later usage of the transmittance shapes. Some such quantities will be described in the next section.

3.4.6. Common statistics

When a satisfactory fit was not achieved using the provided shapes, an alternative approach was employed to extract the required information directly.

The FWHM was estimated by locating the indices where the data falls below half of the maximum value on both sides of the peak. The peak area was estimated by integrating the observed data using the trapezoidal rule.

The CWL was calculated by taking the weighted intensities average of the wavelength values. Lastly, the intensity value at the CWL was extracted based on the calculated index.

The mathematical algorithms related to this can be found in 9.1.7.

For example, Table 9-17 shows the error in percentage for some spectra. It determines that no peak shape satisfactory fits the spectra, so the peak parameters were extracted from the spectra. Figure 3-11 depicts an “arbitrary” spectrum. (used in Chapters 4.5 and 4.8).

Figure 3-11 Recorded spectrum.

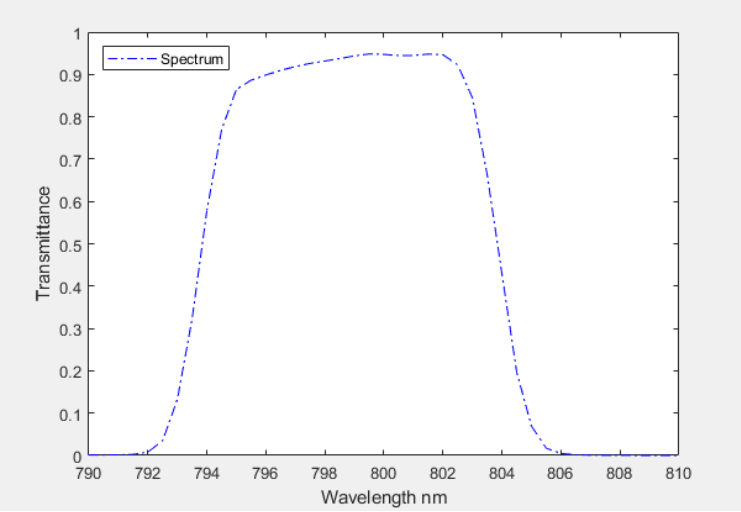

4. CHARACTERIZATION MEASUREMENTS

The actual characterization measurements performed in the framework of current theses will be described in this chapter. The measurements follow the general guidelines [9] and experience from running the “standard setup”. The subchapters describe individual measurement techniques. The results will be presented in the next chapter.

4.1. Effect of monochromator's self-heating on its wavelength setting accuracy

The transmittance measurements' accuracy depends on the monochromator's ability to tune to the specific CWL. However, monochromator self-heating can impact the tuning accuracy. This experiment aimed to investigate the effect of monochromator self-heating on wavelength setting accuracy using a Kr lamp at 0'th order and 785 nm. The PMT detector was used, with a voltage of 250V at 0'th order and 500V at 785 nm. The bandwidth was constant at 0.20 nm.

The experiment was conducted by recording spectra using a PMT detector. The monochromator does not include any thermal control nor temperature sensors installed. Still, it is known that the thermal expansions due to the power dissipation of the scanning motors can affect the wavelength settings [9]. So, the self-heating of the monochromator was used to change its internal temperature. This is sufficient because the characterization conditions should be close to the standard usage. The ambient temperature was 21±0.5 °C.

After switching off the monochromator overnight, it was turned on, and spectra were recorded continuously. The process involved alternating between 0'th order and 785 nm and taking five readings for each wavelength. One spectrum was recorded for each wavelength after 10 minutes, with the time window gradually increasing to 30 minutes. The final spectrum was recorded 6 hours after switching on the monochromator. Twenty spectra were recorded for each line. The schematic of the experiment is shown in Figure 4-1.

Figure 4-1 The schematic of the measurement setup

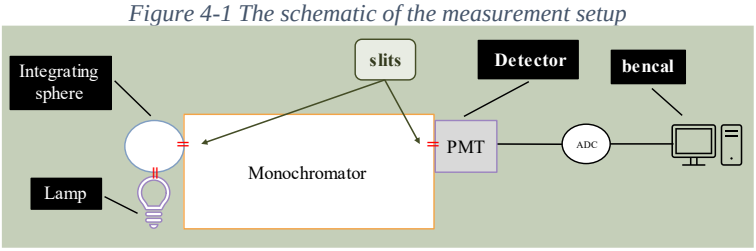

4.2. Effect of monochromator Bandwidth setting on the apparent resolution

The resolving power in equation 3-1 is the monochromator's main parameter for the spectral measurements. The DTMS300 monochromator allows automatically sets the desired bandwidth for each individual CWL. The bandwidth $\Delta\lambda$ is calculated as:

$$\Delta\lambda = \Delta x \times \frac{d\lambda}{dl}$$

where Δx is the slit width in mm, and $d\lambda/dl$ is the reciprocal linear dispersion in nm/mm [23]. However, due to the non-ideality of the components, the real (apparent) bandwidth can be somewhat different from the reported one. In order to retrieve the apparent bandwidth, the monochromator is scanned over the sufficiently narrow input line. The pen-ray lamps [16] and gas discharge lasers [24] provide spectral lines of widths below 0.001 nm and are sufficient for that task.

This experiment investigated the impact of monochromator bandwidth on peak resolution using three lamps: Hg lamp at 0'th order, 297 nm, 495 nm, and 546 nm, HeNe laser at 0'th order and 633 nm, and Kr lamp at 0'th order, 785 nm, and 877 nm.

The experiment was carried out by recording the spectra of each emission line using a PMT detector. The Si diode was insufficiently sensitive. The integrating sphere was used when illuminating the entrance slit. The PMT anode voltage was adjusted to 500 V for weak lines and 250 V for the rest. The monochromator bandwidth was changed from 0.05 nm to 3.00 nm for each lamp line, and the spectra were recorded. The schematic of the experiment is shown in Figure 4-1.

4.3. Spatial non-uniformity of the radiation field at the detector's plane

The effect of the detector's horizontal movement on the output signal was investigated. This is particularly important as mimicking the error due to the misalignment of the detector during repeated installation. Repeated installation is part of the standard measurement procedure. The detector was moved (Figure 4-2) horizontally, and its output signal was recorded. The signals from RFL at 555 nm and the Hg at 546 nm were measured. The RFL was used to detect the change in absolute signal value, and Hg was used to detect the shift of apparent CWL. The recordings were conducted using the 'bencal' software, which captured the spectrum ten times at each WL and calculated an average. The software automatically subtracts the intensity of dark mode, eliminating background noise or interference. The BW was constant at 1.00 nm.

In the case of RFL, ten intensities were recorded at 555 nm. The dark mode intensities were subtracted to remove any background noise or interference. The BW used in the measurement was constant at 1.00 nm. The signal intensity was detected using a silicon diode with a 3 mm aperture (see 3.1.4).

Figure 4-2 The schematic of the experiment while the detector is moved horizontally (a) set up (b) taken from above (c) side view.

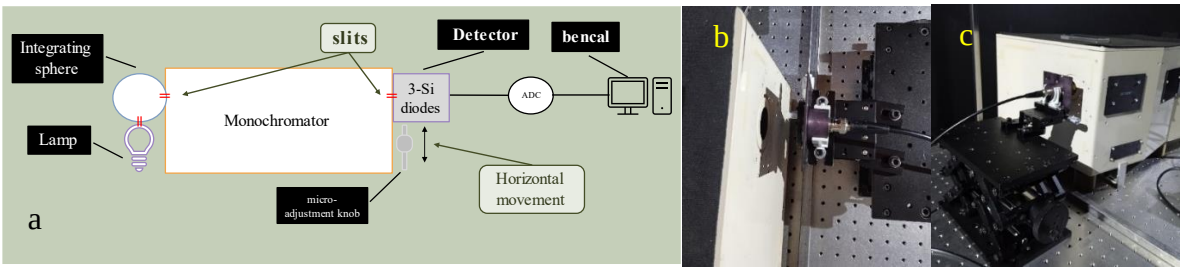

The “standard alignment” (chapter 4.5) was used, yielding the detector's horizontal position of 0 mm. At first, the signal level at 0 mm was recorded, followed by moving the detector horizontally at -1 mm, -0.5 mm, 0.5 mm, and 1 mm and then again at 0 mm deviation. Returning to the initial position was needed to characterize the possible lamp’s intensity drift during the experiment.

4.4. Spatial non-uniformity and CWL shift at the detector's plane

As known in the case of a double monochromator with added dispersions [11], the signal at the exit slit has dispersion along the wavelength. In order to investigate the apparent intensity and CWL changes at the detector's plane simultaneously, the technique in the previous section was modified. An array spectroradiometer was used instead of the silicon diode, allowing retrieval of both the spectral and intensity data. The spectrometer was a Wasatch WP-VISNIR-R2-IC OEM (3.2.8). FOV of the input fiber was limited by a ø3 mm aperture, imitating the geometry of the “standard setup”.

The effect of the detector's spatial movement on the detected peak wavelength and signal intensity was investigated. To do so, the spectrometer was moved horizontally and vertically (Figure 4-2 and Figure 4-3) to quantify the positioning error. The Kr emission lines 380 nm, 550 nm, and 800 nm were used. The whole time BW was constant at 1.00 nm. The fiber input was initially aligned to the 0 mm position according to the “standard alignment” procedure.

Figure 4-3 The schematic of the experiment while the detector is moved Horizontally and Vertically.

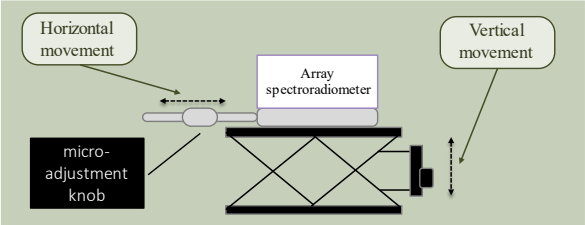

First, the spectrum at the 0 mm position was recorded. Then, the measurement was repeated, moving the detector horizontally at -2 mm, -1 mm, -0.5 mm, 0.5 mm, 1 mm, and 2 mm and then again at 0 mm deviation. Then the detector was moved vertically to -2 mm, and the measurement was repeated. Next, it was moved to the +2 mm vertically, and the measurement was repeated. Then, it was moved to zero horizontally and vertically, and the spectrum at normal and dark modes was recorded. Returning to the initial position was needed to characterize the possible lamp drift during the experiment.

The readings were taken semi-manually as the WASATCH spectrometer is not integrated into the standard setup. Recordings were done so that the monochromator's shutter was first closed, and five dark spectra were recorded. Then the shutter was opened (normal mode), and the recordings were repeated five times for each horizontal position. Then, the dark spectra were re-recorded five times (at only 0 mm horizontal deviations). Then, the measurements were repeated for all emission lines.

4.5. Effect of the alignment

The alignment is crucial to ensure accurate spectral measurements. Correct alignment of the measurement system can help to prevent deviations in the central wavelength, resulting in consistent and precise measurements.

Defining the optical axis in Figure 3-1 is not exclusive. The optical axis can be defined with the help of a laser beam hitting the center of one slit and exiting the center of the opposite slit. The easiest way is to rotate the gratings so that the 0'th order diffraction passes the monochromator. When placing the mirror in the way of the laser beam, the beam should travel back to the laser. Due to the slight misalignment of the monochromator's internal mirrors and gratings, at least four external alignment cases are occasionally used and have to be analyzed (Figure 4-4). In addition, the integrating sphere option, used during the wavelength calibration of the monochromator, has to be included as well.

Figure 4-4 The four external monochromator's alignment

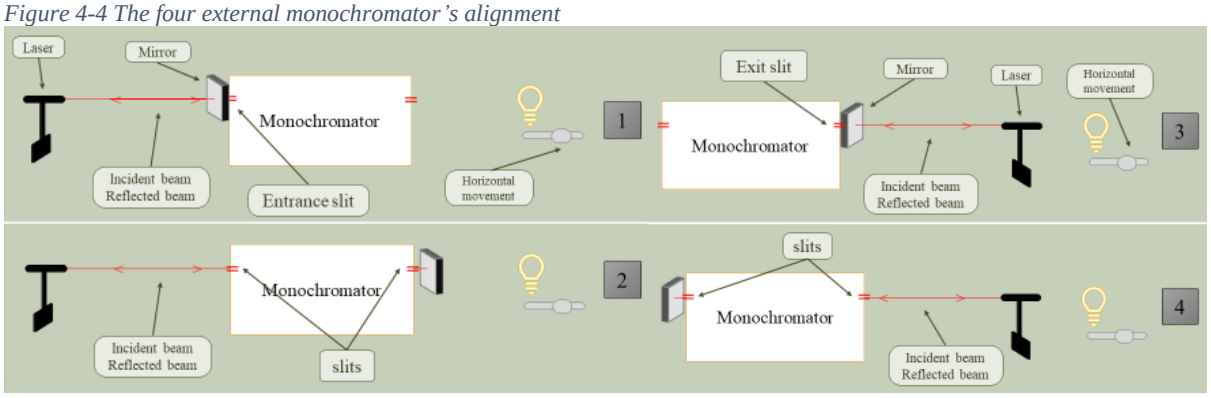

The alignment types are arbitrarily numbered from #1 to #4. In order to perform reliable transmittance measurements with the standard setup (Figure 3-1), the "standard alignment" has to be defined. As the filter radiometer is fixed at the exit slit of the monochromator, case #2 is chosen as the "standard". Most of the characterization measurements in this document are referenced to the standard alignment.

In cases #1 and #3, the mirror is placed on the slit closest to the laser. In cases #2 and #4, the beam is reflected back from the opposite slit. The laser's position is chosen so that the reflected beam returns to the laser. All 4 cases yield different laser beam positions at the lamp's plane. As the apparent wavelength at the exit slit depends on the optical axis, the four optical axes were determined experimentally.

For the alignment, the laser beam was pointed to the slit through a target made of graph paper. In the center of the target, there was an opening for the incident laser beam. The position of the back-reflected beam was marked directly on the target (see Figure 9-7). The angular and linear positions (see 9.3.2) are relative to the standard setup #2.

After determining the four lamp positions, the pen-ray lamp and detector were installed, and selected emission lines were scanned. The 1 nm BW was used to closely mimic the standard transmittance measurement conditions. At last, the integrating sphere was installed at the entrance slit, and the same emission lines were scanned again. The apparent CWL was calculated using the Gaussian fitting method. The measurement geometry is illustrated in Figure 9-7.

Then the deviation angles for each lamp position with respect to #2 were calculated. (9.3.2)

4.6. Inhomogeneity of the light field

The Ribbon Filament lamp scatters light inhomogeneously. Investigating the inhomogeneity, the proposed experiment was conducted. The lamp was aligned according to the standard

method #2. The 3-Si trap detector was placed on the translation table, allowing vertical movement. The initial position was determined by the alignment laser and considered the zero position. Then from -2 mm to 2 mm deviations from the zero position were used to record the intensity. The monochromator was set at 555 nm CWL and 1.00 nm bandwidth. The data was recorded by using the Bencal program. Five data series were recorded. The dark signal was subtracted accordingly. Then, the signal average at each position was calculated and normalized to the zero-position value.

4.7. The Slit Scattering Function

The slit scattering function (SLF) measures a monochromator's ability to resolve narrow spectral lines by describing the spectral intensity distribution at the exit slit when radiation of very narrow BW enters the monochromator. The reasons for spectral scattering were introduced in 3.3. The SLF can be expressed as the product of two components: the responsivity factor $R_f(\lambda')$, which depends solely on the wavelength of the incident light and the slit function $Z(\lambda_0, \lambda')$, which contains all the dependence on the instrument wavelength setting λ_0 and is arbitrarily normalized to unity at $\lambda' = \lambda_0$ [22]. To do so, a narrow spectral line, such as a dye laser, is passed through the monochromator. The excitation is scanned over the wavelength range of interest I' while the output signal is recorded at the wavelength setting I_0 [9].

In practice, the inverse process is usually carried out, in which the source wavelength is fixed, and the monochromator is scanned through a range of wavelength settings. This is easier to perform and does not require knowledge about the intensity of the incident radiation. It is shown [7] that the direct and inversed methods give coinciding results down to the 10^{-7} signal level, which is sufficient in our case.

Attempts to determine the slit scattering function for double monochromators are rare. Saunders and Shumaker [22] studied the slit function of a prism-grating double monochromator used in the NIST's FASCAL system using a dye laser and a few ion laser lines. The value of the slit function was found to be about nine orders of magnitude below the peak at 300 nm from the line center.

In this experiment, the LT52 laser with a wavelength of 655 nm (3.2.2) was first used. Due to the low wings of the SLF (Figure 4-5), the PMT was the detector of choice. The spectral range was divided into three parts. Around the peak, the output signal was scanned with a 0.2 nm step, and an anode voltage of 250 was used. Outside the central peak, the signal was scanned with a 10 nm step, and PMT's anode voltage of up to 750 V was used.

Moreover, the dark spectra at 250 V and 750 V were recorded and subtracted from the spectra, and the ratio of the remaining spectra at 750 V over 250 V was calculated. The amplification factor between the 250 V and 750 V anode voltages was determined directly at a constant wavelength near the central peak. The schematic of the experiment is depicted in Figure 4-5. Then, the experiment was repeated using the HeNe laser with a wavelength of 633 nm.

The SLF is calculated in Chapter 5.6.

Figure 4-5 The schematic of the measurements

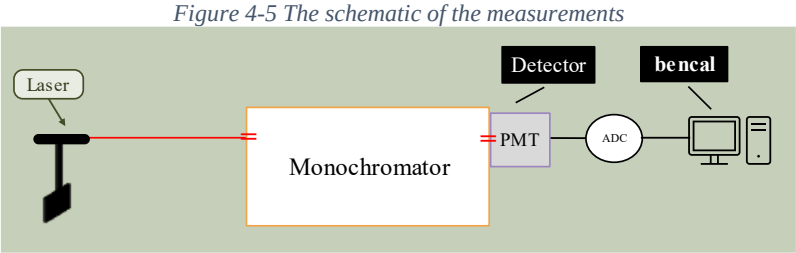

4.8. Effect of filter's Temperature on transmittance

The filter transmittance depends on the temperature. Especially sensitive are the interference filters for which both the cut-off wavelengths and transmittance can vary significantly. As the ~10 nm FWHM interference filters are used in the filter radiometer for methods M804-M806, direct determination of the temperature sensitivity was determined in the case of two filters (CWLs of 380 nm and 800 nm, respectively).

This experiment investigated the effect of the filter's temperature in the “standard setup” (Figure 3-1).

Two narrow-band interference filters with CWLs of 360 nm and 800 nm were investigated. The typical transmission curves of the filters are shown in Figure 5-7. The monochromator was scanned over the transmittance region of the filters. The scans were performed at filter temperatures of 25 °C, 18 °C, 32 °C, and again at 25 °C. The reference spectra with an empty filter holder were recorded for each filter twice. Dark readings were measured and subtracted automatically. The data treatment involved dividing the spectra by the reference for each wavelength in order to derive the spectral transmittance *T*. The average transmittance at 25 °C spectrum was considered as the reference. Then, the transmittance ratio at each temperature over the first 25 °C was calculated. The whole time BW was constant at 1.00 nm.

4.9. Transmittance measurement

In order to validate the uncertainty budget and get the actual reproducibility, the transmittance of one neutral density optical glass filter and one narrow band interference filter were measured

according to the method M807 [10]. The measurement consists of multiple sequential scans of the filter and reference. During this, the filter was repeatedly replaced with the empty filter holder, and the radiometer was re-attached to the monochromator. The transmittance was calculated as the ratio of the neighboring filter and reference scan pairs. The standard measurement setup was used with a 1 nm bandwidth. The transmittance values were used directly for the neutral density filter. Centroid wavelength and area under the transmittance curve (chapter 3.4.6) were evaluated for the interference filter.

5. RESULTS AND DISCUSSION

5.1. Thermal stability of the wavelength scale

The wavelength scale is the main parameter that the monochromator provides for spectral measurements. The wavelength scale is periodically checked against the line sources [10]. The residual bias, repeatability, and especially the temperature response determine the uncertainty caused by the wavelength scale. The manufacturer specifies the bias and repeatability. The thermal change was determined experimentally, as described in 4.1.

Individual spectral lines were scanned after switching on the monochromator, and the CWLs were calculated. Figure 5-1 shows the apparent change of CWL referenced to the median at 0'th order and 785 nm. The spectra were fitted to Flattened Gaussian peaks.

Figure 5-1 The apparent CWL shift during monochromator warm-up.

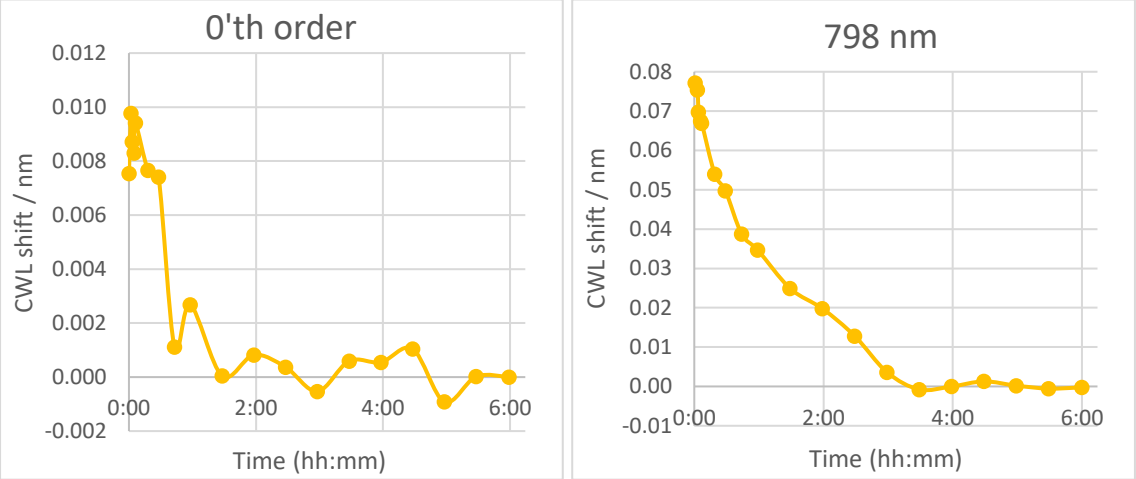

Figure 5-1 shows that:

- For the 0’th order: the CWL shifted to the shorter WLs by passing the time. At first, it has a steeper slope but gradually reaches a stable level, so it does not shift considerably after one hour and a half after the first measurement. The overall shift is 0.02 nm, below the specified wavelength setting error of the monochromator.
- For 785 nm: the CWL shifted to the shorter WLs by passing the time. At first, it has a steeper slope but gradually reaches a stable level, so it does not shift considerably after three hours and a half of the first measurement. The shift is 0.1 nm, comparable to the monochromator's specified wavelength accuracy.

It is clear from Figure 5-1 that the monochromator should be warmed up for almost 4 hours before performing the calibration measurements, including calibration of the monochromator's

wavelength scale. After 4 hours, the CWL shift will not contribute significantly to the uncertainty budget of the transmittance measurement. These considerations will be added to the method M807.

5.2. Reported vs. apparent bandwidth.

The slit widths of the DTMS300 monochromator are continuously calculated and set by the software considering the linear dispersion. We refer to this as the reported BW. The apparent BW was found by scanning sufficiently narrow (<0.01 nm) spectral lines. The lines were fitted to the Gaussian shape, and the FWHMs of the peaks were calculated.

The experiment results confirmed a linear relationship between the reported and apparent bandwidths at tested wavelengths. The HeNe graph at 633 nm is shown in Figure 5-2, with reported BW on the x-axis and apparent on the y-axis. The fitting parameters are reported in Table 5-1. The slope of the relationship is close to 1. The intercept of the relationship reflects the normal slit width. According to the grating data, the normal width cannot be smaller than 0.05 nm [11]. Determined from our measurements, 0.07 nm agrees well with that and shows that the alignment of the monochromator's internal components is satisfactory.

Figure 5-2 The relationship between the reported and apparent BW for the HeNe laser at 633 nm fitted to Gaussian peak shape.

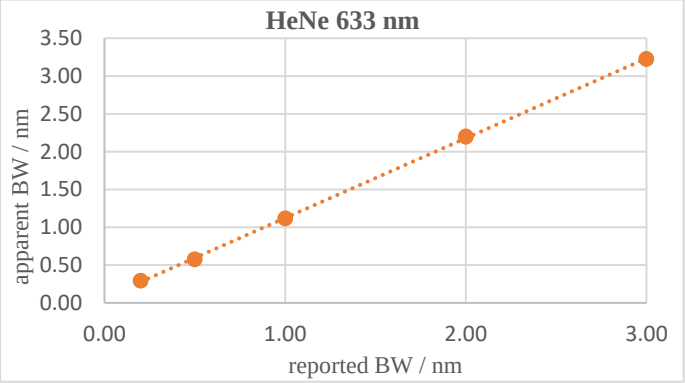

Table 5-1 The fitting parameters for the HeNe laser at 633 nm

Slope = 1.06 ± 0.01	Intercept = 0.07 ± 0.01

5.3. Non-uniformity of the radiation field at the detector's plane

This is amongst the main contributors to the transmittance uncertainty budget. The non-uniformity is mainly caused by the insufficient alignment of the monochromator and by optical aberrations. Three experiments were conducted to characterize the spatial non-uniformity. First (4.3), the apparent signal level at a fixed wavelength was determined when moving the spectrally non-sensitive detector (a silicon diode) in the light field behind the exit slit. The RFL was

the light source. This should mimic the standard measurement setup in terms of the detector part. Then the shift of apparent CWL was measured using the Hg pen-ray lamp.

Third (4.4), the light field was characterized with the fiber-coupled spectroradiometer. The ribbon filament lamp was used in standard configuration. Thanks to thermal stabilization, the Wasatch spectroradiometer is stable enough to determine the absolute value and CWL of the scan simultaneously. The detector's input was equipped with a ø3 mm aperture in all three cases.

The intensity change of the RFL light field depending on the detector's position was measured with the Si detector. The apparent CWL shifts were determined for the Hg well-isolated 546.1 nm emission line using the Si detector. The spectra were fitted to a Gaussian shape. With the spectroradiometer, the light field of the RFL was measured at 380 nm, 550 nm, and 800 nm. The scans were fitted with the Gaussian shape. As the signal intensity measure, the peak area was used.

The Si-diode detector head was moved in the direction perpendicular to the slit, the x-direction. The fiber end was moved in both the x and y directions. The zero coordinate corresponds to the alignment method #2 in Chapter 3.3.

Figure 5-3 shows that the CWL for the Hg 546.1 nm line changes for approx. 0.03% when moving the detector within ±2 mm around the aligned position. After finding the average highest intensity without background for each position, they were divided by the first 0 mm deviation to find the ratio. Next, the graph was plotted, shown in Figure 5-3, with the horizontal deviation in mm on the x-axis and the averaged highest intensity ratio on the y-axis. Figure 5-4 shows the change of the apparent CWL and intensity when moving the fiber head of the spectrometer in both the x and y directions for 550 nm (for 380 nm and 800 nm, the results are similar). The measurement points are fitted with low-order polynomials for better readability. The apparent CWL stays within 0.04%, and the signal intensity is within 10% for the movements within 2x2 mm.

Figure 5-3 The relationship between CWL and horizontal deviation of the detector for the Hg lamp at 546.1 nm (left); and the relationship between max intensity and horizontal deviation for RFL at 555 nm (right).

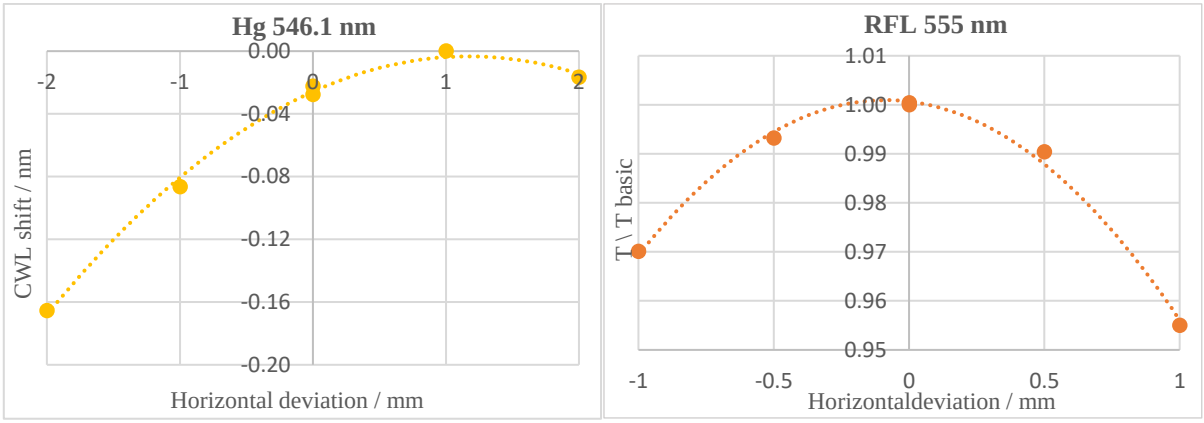

Figure 5-4 The CWL and peak area related to filter 550nm at spatial deviation The relationship between CWL and horizontal deviation (left), and peak area and horizontal deviation (right) for Kr lamp and three different vertical positions.

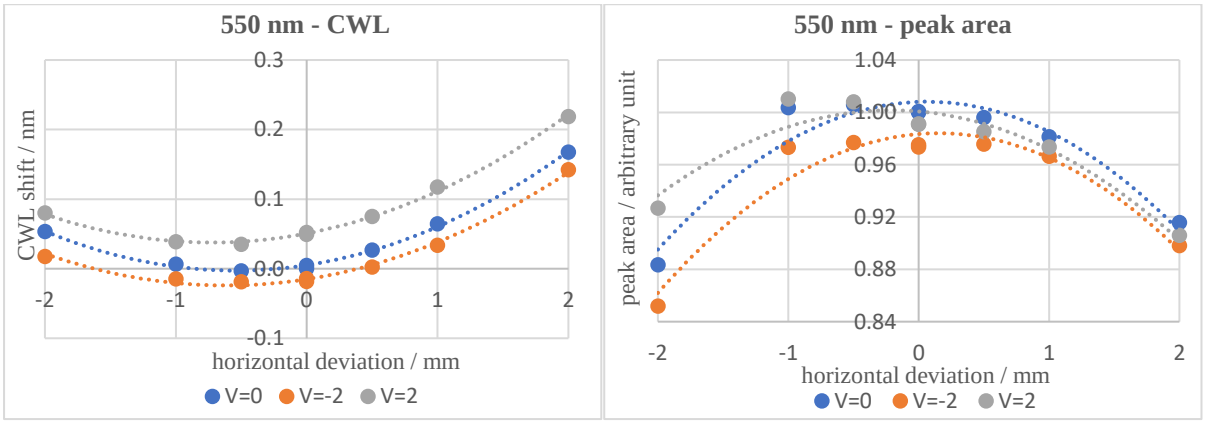

The graphs show that as the detector was moved away from the optimal position, the intensity ratio decreased following a parabolic curve. It is evident from the graph above that uncertainty due to the alignment error of ± 0.2 mm stays within 0.2% and the apparent CWL shift within 0.05 nm.

5.4. Sensitivity to the alignment method

As explained in Chapter 4.5, the alignment of the measurement setup is not exclusive [10] and has to be explicitly defined. There are four alignment options, and we call option #2 “standard” because it is the one used during the transmittance measurements. In addition to this, the integrating sphere is used to calibrate the monochromator's wavelength scale.

In order to quantify differences between the alignments, the apparent CWLs of the emission lines were used. First, the lamp positions for all four alignment methods were determined using an alignment laser, as described in Chapter 4.5. Then, the pen-ray lamps were placed in these four positions, and apparent CWLs of selected emission lines were determined. In addition, the

5th alignment with the integrating sphere was used. The spectral lines were fitted with the Flattened Gaussian shape.

The apparent CWLs, along with the lamp positions in terms of linear and angular displacements for all alignments options, are given in 9.3.2. The maximum difference of 0.07 nm is at 877 nm between alignment options #1 and #2. The CWL differences between the standard alignment setup #2 and the sphere setup reach 0.02 nm. The latter result contributes directly to the uncertainty budget of the transmittance measurement as it shows the difference in the monochromator's wavelength scales between the calibration and transmittance measurements. This value will be added to the uncertainty budget. However, the values are negligible compared to the wavelength setting errors of ~ 0.1 nm.

5.5. Inhomogeneity of the light field

An attempt was made to detect the spatial inhomogeneity of the RFL filament image, as described in Chapter 4.6. The vertical scan results of the light field in the detector's plane are shown in Figure 5-5. The data is presented as integral intensity vs. the detector position.

Looking at the data, it is clear that:

- the spatial non-uniformity, although visually detectable on the filament, cannot be detected at the detector plane because of aberrations and slight de-focusing and that
- the vertical non-uniformity exists and has to be added to the uncertainty budget.

Figure 5-5 The relationship between the Integral intensity and detector position for RLF

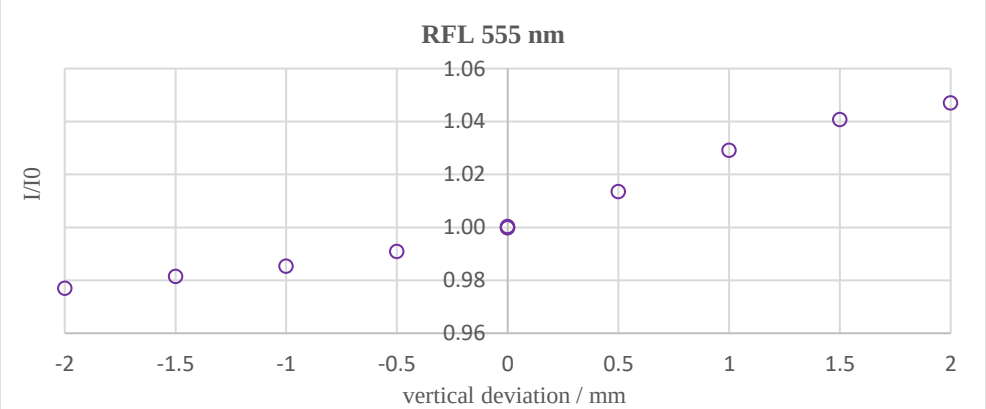

As the uncertainty of the vertical alignment with the current setup stays within ± 0.1 mm, we add, according to Figure 5-5, 0.2% of the vertical alignment uncertainty to the budget. The uncertainty is essentially caused by the repeated attachment of the filter radiometer during the transmittance measurement.

5.6. The slit scattering function

The slit scattering function was measured for two laser lines according to the methodology in 4.7. The results are depicted in Figure 5-6. The out-of-band rejection is at least seven orders of magnitude and is mainly limited by the detection electronics. The reported results [9] [22] for double monochromators vary between 6 and 10 orders of magnitude. Using the SLF and convolution techniques are out of the scope of the current thesis and are described elsewhere [9] [20]. The effect of the finite out-of-band rejection depends on the filter transmittance: the steeper the transmittance slope, the higher the effect. In the cases of slowly changing signals (the reference line or transmittance of the colored glass filters), the stray light effect can be ignored completely. In the case of narrow-band interference filters, the effect is evaluated individually.

In overall, the slit-scattering function provides essential information about the performance of a monochromator or spectrometer and is a critical factor in ensuring accurate and precise measurements in spectroscopy. The deconvolution techniques, taking into account the monochromator's stray light, are briefly introduced in Appendix 9.5.

Figure 5-6 The slit scattering function for HeNe and LT52 lasers.

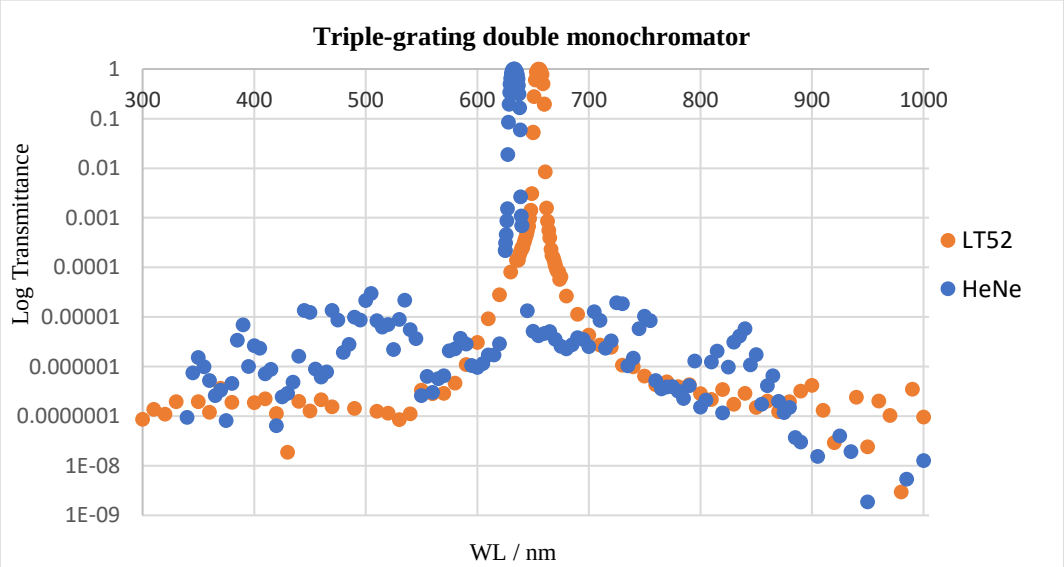

5.7. Temperature sensitivity of the transmittance

This component is related to the object itself, i.e., to the filter under calibration. Handling the filter's thermal properties is not straightforward in general, as it requires knowledge of the latter usage of the filter. However, in the case of filter radiometer type HHFR03-S1337, the corresponding uncertainty can be directly evaluated as the filters are always used in well-defined environmental conditions. The transmittance of two typical interference was determined at

18 °C, 25 °C, and 32 °C as described in 4.8. Based on the scan results, the CWL-s and areas under the transmittance curves were calculated as these two quantities are most related to the later use of the filters in methods M804-M806. The CWL was calculated as a centroid value (9.1.7). The area was calculated according to 9.1.

Figure 5-7 The relationship between T at different T°C/ T at first 25°C and WL nm for the Ribbon filament lamp at (a) 360 nm (b) 800 nm.

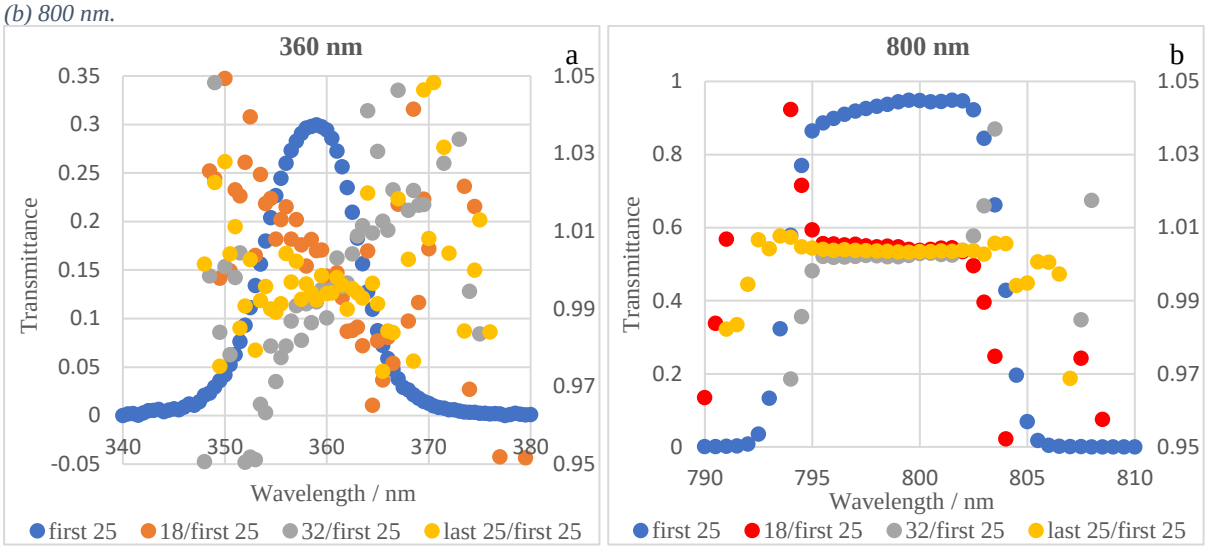

Plotting those ratios in Figure 5-7 shows that:

- *T* at 18 °C/ *T* at first 25 °C: the peak shifted to shorter wavelengths for both filters.
- *T* at 32 °C/ *T* at first 25 °C: the peak shifted to longer wavelengths for both filters.
- *T* at last 25 °C/ *T* at first 25 °C: the data scattered around 1, so the temporal drift was insignificant.

The data analysis obtained for 360 nm and 800 nm shows a clear close to linear relationship between CWL and temperature, as depicted in Figure 5-8. The results indicate that as the temperature increases, the CWL also increases, resulting in a shift towards higher wavelengths for both lines.

The change of the calculated area with temperature is shown in Figure 5-9. The results indicate that as the temperature increases, the peak area decreases.

The filter temperature during the transmittance measurements is expected to stay within ± 0.2 °C [25]. This corresponds to the transmittance uncertainties of 0.02 nm (CWL) and 0.002% (area) for the selected filters. These results are individual to the filters, will be determined separately, and do not contribute to the M807 uncertainty budget in general.

Figure 5-8 The relationship between CWL and T for the Ribbon filament lamp and fitted spectra and parameters.

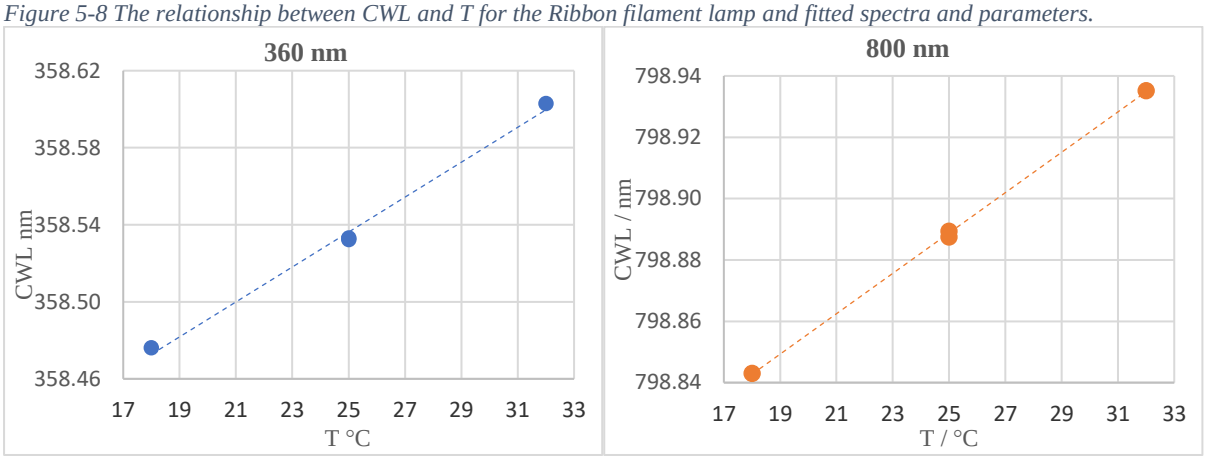

Filter 360 nm	slope = 0.0091 ± 0.0005	Intercept = 358.31 ± 0.021
Filter 800 nm	slope = 0.0066 ± 0.0001	Intercept = 798.724 ± 0.003

Figure 5-9 The relationship between peak area and T for the Ribbon filament lamp and fitted spectra and parameters.

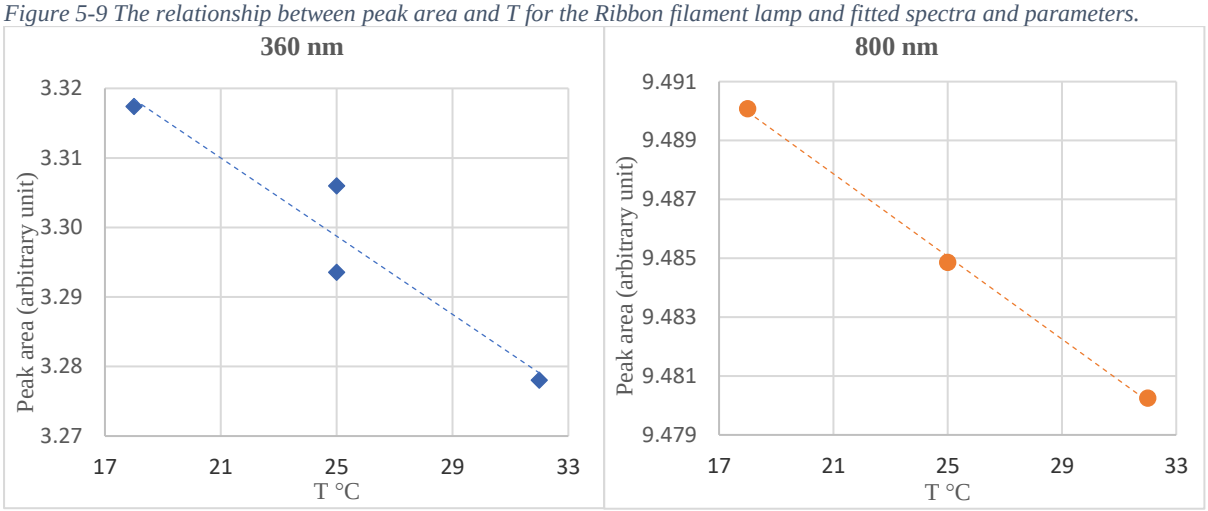

Filter 360 nm	slope = -0.0028 ± 0.0006	Intercept = 3.37 ± 0.02
Filter 800 nm	slope = -0.00070 ± 0.00002	Intercept = 9.503 ± 0.001

5.8. Reproducibility

The results of reproducibility of the spectral transmittance measurements (4.9) for the neutral density filter are presented in Figure 9-8. For the narrow-band interference filter, the reproducibility of CWL is 0.0023 nm, and the reproducibility of shape area is 0.11%. The reproducibility shows the theoretically lower limits of the uncertainties for the calculated parameters when all the systematical components are removed or corrected. The results are coherent with the current experience with transmittance measurements according to method M807. These results contribute to the uncertainty budgets of methods M804- M807.

5.9. Method update

According to the results of this work, the uncertainty budget of the method M807 is modified with detailed contributions from the spatial and wavelength accuracy.

The following general updates and recommendations were proposed:

- Introduce clear requirements of warm-up time for the transmittance and calibration measurements. Suggest installation of the temperature sensors inside the monochromator.
- Switching to the double monochromator with subtracted dispersion [9]. This will help to reduce the uncertainty components related to wavelength spatial distribution at the detector's plane. The current thesis can be directly used when characterizing the new monochromator.
- Update the wavelength calibration procedure to be closer to the standard alignment. This would further reduce the wavelength scale shift between the calibration and transmittance measurements.

6. SUMMARY

During this study, a comprehensive characterization of an accredited filter transmittance measurement setup M807 was performed. The thesis includes a description of the measurement and characterization instrumentation, the measurement procedures, data analysis, and conclusions. Updates to the method's document were proposed.

7. ACKNOWLEDGEMENTS

I would like to express my gratitude to Prof. Riho Vendt for providing me with the opportunity to work with his professional group and for his support throughout my thesis.

I am also thankful to Prof. Ivo Leito for his crucial role in guiding me and enabling me to reach the point of defending my thesis.

I would like to acknowledge the kind students from EACH 2021 who were always there to help me. Their support has been invaluable.

8. REFERENCES

[1] A. Höpe, "Chapter 6 - Diffuse Reflectance and Transmittance," *Academic Press,*, vol. 46, pp. 179-219, 2014.

[2] H.-J. Hoffmann, "Optical Glasses," *Encyclopedia of Materials: Science and Technology,Elsevier,*, pp. 6426-6441, 2001.

[3] D. R. Paschotta, "RP Photonics Encyclopedia," [Online]. Available: https://www.rp-photonics.com/optical_intensity.html.

[4] "Acoustic resonance spectroscopy," Wikipedia, the free encyclopedia, [Online]. Available: https://en.wikipedia.org/wiki/Acoustic_resonance_spectroscopy.

[5] "Fluorescence spectroscopy," Wikipedia, the free encyclopedia, [Online]. Available: https://en.wikipedia.org/wiki/Fluorescence_spectroscopy.

[6] C. n. ND-ONE-W, "NanoDrop™ One/OneC Microvolume UV-Vis Spectrophotometer," Thermo Fisher Scientific, [Online]. Available: https://www.thermofisher.com/order/catalog/product/ND-ONE-W.

[7] P. K. e. al, "Filter radiometry based on direct utilization of trap detectors," *Metrologia* , vol. 35, p. 255, 1998 .

[8] S. S. Instruments, "What is a diode array spectrophotometer?," Shimadzu , [Online]. Available: https://www.ssi.shimadzu.com/service-support/faq/uv-vis/instrument-design/18/index.html.

[9] H. J. Kostkowski, "Spectral Scattering," in *Reliable spectroradiometry*, La Plata, Maryland 20646-2747, USA, Spectroradiometry Consulting, 1997, p. 609.

[10] I. Ansko, "M807 Calibration of filter transmittance," TESTING CENTRE of University of Tartu , Tartu, 2022.

[11] Bentham, "DTMS300 Double Monochromator," Bentham, [Online]. Available: https://www.bentham.co.uk/products/components/dtms300-double-monochromator-41/.

[12] "Silicon photodiode absolute spectral response self-calibration," Trap detector, [Online]. Available: https://doi.org/10.1364/AO.19.001214.

[13] "Si Photodiodes," Hamamatsu, [Online]. Available: https://www.hamamatsu.com/content/dam/hamamatsu-photonics/sites/documents/99_SALES_LIBRARY/ssd/si_pd_kspd9001e.pdf.

[14] H. OÜ, "FILTER RADIOMETER FOR SPECTRAL IRRADIANCE SCALE IN THE WAVELENGTH RANGE FROM 440 nm TO 950 nm," Project Interim (November 2011) Report.

[15] "Temperature controller Newport Corporation 350B," [Online]. Available: https://www.newport.com/f/laser-diode-temperature-controller-350b.

[16] L.-O. G. Europe, "Light sources for calibration Pen-Ray line sources for wavelength calibration," LOT-Oriel Group Europe.

[17] "Integrating Sphere Theory and Applications," Labsphere, [Online]. Available: https://www.labsphere.com/wp-content/uploads/2021/09/Integrating-Sphere-Theory-and-Applications.pdf.

[18] W. Kester, "ADC Architectures III: Sigma-Delta ADC Basics," Analog Devices, [Online]. Available: https://www.analog.com/media/en/training-seminars/tutorials/MT-022.pdf.

[19] "Photomultiplier Tubes Handbook (4th ed.)," Hamamatsu Photonics K.K., [Online]. Available: https://www.hamamatsu.com/content/dam/hamamatsu-photonics/sites/documents/99_SALES_LIBRARY/etd/PMT_handbook_v4E.pdf.

[20] A. B. J. K. Ilmar Ansko, "MetEOC-3," Tartu University, NPL, Tartu, 2021.

[21] "Resolvance of Grating," hyper physics Georgia State University, [Online]. Available: http://hyperphysics.phy-astr.gsu.edu/hbase/phyopt/gratres.html.

[22] R. D. S. a. J. B. Shumaker, "Apparatus function of a prism-grating double monochromator," *APPLIED OPTICS,* p. 5, 1986.

[23] A. C. P. a. K. B. Thomas Lucatorto, Experimental Methods in the Physical Sciences, vol. 46, Elsevier, 2014.

[24] E. Hecht, Optics, Adelphi University, 2017.

[25] Hohenheide, "Temperature stabilisation study of filter holder by using temperature controller".

[26] "Journal of Physics: Conference Series," characterization of spectral irradiance system, [Online]. Available: https://iopscience.iop.org/article/10.1088/1742-6596/733/1/012037/pdf.

[27] "Measuring Laser Beam Divergence," U.S.LASER corporation, 20 11 2015. [Online]. Available: https://web.archive.org/web/20151120123452/http://www.uslasercorp.com/envoy/diverge.html.

[28] T. Observatory, "FILTER RADIOMETER FOR SPECTRAL IRRADIANCE SCALE IN THE WAVELENGTH RANGE FROM 440 nm TO 950 nm," Hohenheide OÜ, 2011.

9. APPENDICES

9.1. MATLAB fitting code

The MATLAB code for fitting the peak was used to fit the spectrum into six peak shapes. The squared mean residual was used to determine the goodness of fit. This code was able to calculate CWL, The highest intensity, FWHM, Peak area, error in percentage, and the squared mean residual:

```
% A command-line peak fitting program for time-series signals, written as a
% self-contained Matlab function in a single m-file. Uses a non-linear
% optimization algorithm to decompose a complex, overlapping-peak signal
% into its component parts. The objective is to determine whether your
% signal can be represented as the sum of fundamental underlying peaks
% shapes. Accepts signals of any length, including those with non-integer
% and non-uniform x-values. Fits any number of peaks of any of 45 curve
% shapes. This is a command line version, usable from a remote terminal. It
% is capable of making multiple trial fits with slightly different starting
% values and taking the one with the lowest mean fit error. It
% can estimate the standard deviation of peak parameters from a single
% signal using the bootstrap method.
%
% peakfit(signal);
% Performs an iterative least-squares fit of a single Gaussian peak to the
% data matrix "signal", which has x values in column 1 and Y values in
% column 2 (e.g. [x y]).
%
% peakfit(signal,center,window);
% Fits a single Gaussian peak to a portion of the matrix "signal". The
% portion is centered on the x-value "center" and has width "window" (in x
% units).
%
% peakfit(signal,center,window,NumPeaks..);
% "NumPeaks" = number of peaks in the model (default is 1 if not
% specified). No limit to maximum number of peaks in version 3.1
%
% peakfit(signal,center,window,NumPeaks,peakshape); "peakshape" specifies
% the peak shape of the model: 1=Gaussian; 2=Lorentzian;
% 20=Voigt profile; 21=triangular; 41=rectangle; 42=flattened Gaussian;
%
% [FitResults,LowestError,BestStart,xi,yi,BootResults]=peakfit(signal,...)
% Prints out parameter error estimates for each peak (bootstrap method).
% Optional output parameters
% 1. FitResults: a table of model peak parameters, one row for each peak,
```

```
%    listing Peak number, Peak position, Height, Width, and Peak area.
% 2. GOF: Goodness of Fit, a vector containing the rms fitting error of the
%    best trial fit and the R-squared (coefficient of determination).
% 3. Baseline, the polynomial coefficients of the baseline in linear
%    and quadratic baseline modes (1 and 2) or the value of the constant
%    baseline in flat baseline mode.
% 4. coeff: Coefficients for the polynomial fit (shape 28 only; for other
%    shapes, coeff=0)
% 5. residual: the difference between the data and the best fit.
% 6. xi: vector containing 600 interploated x-values for the model peaks.
% 7. yi: matrix containing the y values of each model peak at each xi.
%    Type plot(xi,yi(1,:)) to plot peak 1 or plot(xi,yi) to plot all peaks
% 8. BootResults: a table of bootstrap precision results for each peak
%    and peak parameter.

% Copyright (c) 2015, Thomas C. O'Haver
%
% Permission is hereby granted, free of charge, to any person obtaining a copy
% of this software and associated documentation files (the "Software"), to deal
% in the software without restriction, including without limitation the rights
% to use, copy, modify, merge, publish, distribute, sublicense, and/or sell
% copies of the software, and to permit persons to whom the software is
% furnished to do so, subject to the following conditions:
%
% The above copyright notice and this permission notice shall be included in
% all copies or substantial portions of the software.
%
% THE SOFTWARE IS PROVIDED "AS IS", 2WITHOUT WARRANTY OF ANY KIND, EXPRESS OR
% IMPLIED, INCLUDING BUT NOT LIMITED TO THE WARRANTIES OF MERCHANTABILITY,
% FITNESS FOR A PARTICULAR PURPOSE AND NONINFRINGEMENT. IN NO EVENT SHALL THE
% AUTHORS OR COPYRIGHT HOLDERS BE LIABLE FOR ANY CLAIM, DAMAGES OR OTHER
% LIABILITY, WHETHER IN AN ACTION OF CONTRACT, TORT OR OTHERWISE, ARISING FROM,
% OUT OF OR IN CONNECTION WITH THE SOFTWARE OR THE USE OR OTHER DEALINGS IN
% THE SOFTWARE.

MeanFitError=100*norm(yy-model)./(sqrt(n)*max(yy));
area(m)=trapz(xxx+xoffset,height(m)*AA(m,:)); % Compute the area of each component
peak using trapezoidal method
```

9.1.1. FitGaussian

```
function err = fitgaussian(lambda,t,y)
% Fitting function for multiple Gaussian peaks.
global PEAKHEIGHTS AUTOZERO BIPOLAR LOGPLOT
numpeaks=round(length(lambda)/2);
A = zeros(length(t),numpeaks);
```

```
for j = 1:numpeaks,
%    if lambda(2*j)<MINWIDTH,lambda(2*j)=MINWIDTH;end
    A(:,j) = gaussian(t,lambda(2*j-1),lambda(2*j))';
end
if AUTOZERO==3,A=[ones(size(y))' A];end
   if BIPOLAR,PEAKHEIGHTS=A\y';
   else PEAKHEIGHTS=abs(A\y');end
   z = A*PEAKHEIGHTS;
   if LOGPLOT,
    err = norm(log10(z)-log10(y)');
else
    err = norm(z-y');
end
% ------------------------------------------------------------------------
function g = gaussian(x,pos,wid)
%  gaussian(X,pos,wid) = gaussian peak centered on pos, half-width=wid
%  X may be scalar, vector, or matrix, pos and wid both scalar
% Examples: gaussian([0 1 2],1,2) gives result [0.5000    1.0000    0.5000]
% plot(gaussian([1:100],50,20)) displays gaussian band centered at 50 with width 20.
g = exp(-((x-pos)./(0.60056120439323.*wid)).^2);
```

9.1.2. FitLorentzian

```
function err = fitlorentzian(lambda,t,y)
%      Fitting function for multiple lorentzians, lambda(1)=position, lambda(2)=width
%      Fitgauss assumes a lorentzian function
global PEAKHEIGHTS AUTOZERO BIPOLAR LOGPLOT
A = zeros(length(t),round(length(lambda)/2));
for j = 1:length(lambda)/2,
    A(:,j) = lorentzian(t,lambda(2*j-1),lambda(2*j))';
end
if AUTOZERO==3,A=[ones(size(y))' A];end
if BIPOLAR,PEAKHEIGHTS=A\y';else PEAKHEIGHTS=abs(A\y');end
       z = A*PEAKHEIGHTS;
if LOGPLOT,
    err = norm(log10(z)-log10(y)');
else
    err = norm(z-y');
end
% ------------------------------------------------------------------------
function g = lorentzian(x,position,width)
% lorentzian(x,position,width) Lorentzian function.
% where x may be scalar, vector, or matrix
% position and width scalar
% T. C. O'Haver, 1988
% Example: lorentzian([1 2 3],2,2) gives result [0.5 1 0.5]
g=ones(size(x))./(1+((x-position)./(0.5.*width)).^2);
```

9.1.3. FitTriangular

```
function err = fittriangular(lambda,t,y)
%      Fitting function for multiple triangular, lambda(1)=position, lambda(2)=width
%      between the data and the values computed by the current
%      function of lambda.  Fittriangular assumes a triangular function
%  T. C. O'Haver, May 2006
global PEAKHEIGHTS AUTOZERO BIPOLAR LOGPLOT
A = zeros(length(t),round(length(lambda)/2));
for j = 1:length(lambda)/2,
    A(:,j) = triangular(t,lambda(2*j-1),lambda(2*j))';
end
if AUTOZERO==3,A=[ones(size(y))' A];end
if BIPOLAR,PEAKHEIGHTS=A\y';else PEAKHEIGHTS=abs(A\y');end
z = A*PEAKHEIGHTS;
if LOGPLOT,
    err = norm(log10(z)-log10(y)');
else
    err = norm(z-y');
end
% ---------------------------------------------------------------------
function g = triangular(x,pos,wid)
%Triangle function. pos=position; wid=half-width (both scalar)
%trianglar(x,pos,wid), where x may be scalar or vector,
%pos=position; wid=half-width (both scalar)
% T. C. O'Haver, 1991
% Example
% x=[0:.1:10];plot(x,trianglar(x,5.5,2.3),'.')
g=1-(1./wid) .*abs(x-pos);
for i=1:length(x),
if g(i)<0,g(i)=0;end
end
```

9.1.4. FitRectangle

```
function err = fitrectangle(lambda,t,y)
%      Fitting function for multiple rectangle, lambda(1)=position, lambda(2)=width
%      between the data and the values computed by the current
%      function of lambda.  Fitrectangle assumes a rectangle function
%  T. C. O'Haver, May 2016
global PEAKHEIGHTS AUTOZERO BIPOLAR LOGPLOT
A = zeros(length(t),round(length(lambda)/2));
for j = 1:length(lambda)/2,
    A(:,j) = rectangle(t,lambda(2*j-1),lambda(2*j))';
end
if AUTOZERO==3,A=[ones(size(y))' A];end
if BIPOLAR,PEAKHEIGHTS=A\y';else PEAKHEIGHTS=abs(A\y');end
z = A*PEAKHEIGHTS;
```

```
if LOGPLOT,
    err = norm(log10(z)-log10(y)');
else
    err = norm(z-y');
end
% --------------------------------------------------------------------
function g = rectangle(x,pos,wid)
%rectangle function. pos=position; wid=half-width (both scalar)
%rectangle(x,pos,wid), where x may be scalar or vector,
%pos=position; wid=half-width (both scalar)
% T. C. O'Haver, 2016
% Example
% x=[0:.1:10];plot(x,rectangle(x,5.5,2.3),'.')
g=zeros(size(x));
hw=wid./2;
for i=1:length(x),
if x(i)<pos-hw,g(i)=0;end
if x(i)>pos-hw,g(i)=1;end
if x(i)>pos+hw,g(i)=0;end
end
```

9.1.5. FitVoigt

```
function err = fitvoigt(lambda,t,y,shapeconstant)
% Fitting functions for multiple Voigt profile function
% T. C. O'Haver (toh@umd.edu), 2013.
global PEAKHEIGHTS AUTOZERO BIPOLAR LOGPLOT
A = zeros(length(t),round(length(lambda)/2));
for j = 1:length(lambda)/2,
    A(:,j) = voigt(t,lambda(2*j-1),lambda(2*j),shapeconstant)';
end
if AUTOZERO==3,A=[ones(size(y))' A];end
if BIPOLAR,PEAKHEIGHTS=A\y';else PEAKHEIGHTS=abs(A\y');end
z = A*PEAKHEIGHTS;
if LOGPLOT,
    err = norm(log10(z)-log10(y)');
else
    err = norm(z-y');
end
% --------------------------------------------------------------------
function g=voigt(xx,pos,gD,alpha)
% Voigt profile function. xx is the independent variable (energy,
% wavelength, etc), gD is the Doppler (Gaussian) width, and alpha is the
% shape constant (ratio of the Lorentzian width gL to the Doppler width gD.
% Based on Chong Tao's "Voigt lineshape spectrum simulation",
% File ID: #26707
% alpha=alpha
```

```
gL=alpha.*gD;
gV = 0.5346*gL + sqrt(0.2166*gL.^2 + gD.^2);
x = gL/gV;
% sizeabs=size(abs(xx-pos))
% sizegV=size(gV)
y = abs(xx-pos)./gV;
g = 1/(2*gV*(1.065 + 0.447*x + 0.058*x^2))*((1-x)*exp(-0.693.*y.^2) + (x./(1+y.^2))
+ 0.016*(1-x)*x*(exp(-0.0841.*y.^2.25)-1./(1 + 0.021.*y.^2.25)));
g=g./max(g);
```

9.1.6. Fitngaussian (Flattened Gaussian)

```
function err = fitngaussian(lambda,t,y,shapeconstant)
%   Fitting functions for multiple flattened Gaussian peaks.
% T. C. O'Haver (toh@umd.edu),   Version 1.3, October 23, 2006.
global PEAKHEIGHTS AUTOZERO BIPOLAR LOGPLOT
A = zeros(length(t),round(length(lambda)/2));
for j = 1:length(lambda)/2,
    A(:,j) = ngaussian(t,lambda(2*j-1),lambda(2*j),shapeconstant)';
end
if AUTOZERO==3,A=[ones(size(y))' A];end
if BIPOLAR,PEAKHEIGHTS=A\y';else PEAKHEIGHTS=abs(A\y');end
z = A*PEAKHEIGHTS;
if LOGPLOT,
    err = norm(log10(z)-log10(y)');
else
    err = norm(z-y');
end
% --------------------------------------------------------------------
function g = ngaussian(x,pos,wid,n)
%  ngaussian(x,pos,wid) = flattened Gaussian centered on x=pos, half-width=wid
%  x may be scalar, vector, or matrix, pos and wid both scalar
% Shape is Gaussian when n=1. Becomes more rectangular as n increases.
%  T. C. O'Haver, 1988, revised 2014
% Example: ngaussian([1 2 3],1,2,1) gives result [1.0000    0.5000    0.0625]
if n>0,
    g = 1-(10.^-(n.*gaussian(x,pos,wid)));
    g=g./max(g);
else
    g = gaussian(x,pos,wid);
end
```

9.1.7. Common statistics

```
% Find the maximum value and its index
[max_val, max_idx] = max(y);
% Estimate the full width at half maximum (FWHM)
half_max = max_val / 2;
left_idx = find(y(1:max_idx) <= half_max, 1, 'last');
```

```
right_idx = find(y(max_idx:end) <= half_max, 1, 'first') + max_idx - 1;
FWHM = x(right_idx) - x(left_idx);
% Estimate the peak area
peak_area = trapz(x,y);
% Calculate the center wavelength (CWL)
CWL = sum(x.*y)/sum(y);
% Find the index of the element in x that is closest to the CWL
[~, idx] = min(abs(x - CWL));
% Extract the corresponding element from y
y_at_CWL = y(idx);
```

9.2. Instruments document

Table 9-1 The triple grating double monochromator

Equipment name / No	Monochromator	***S8-16***
Manufacturer	Bentham Instruments Ltd	
Type	DTMS300	
Serial No.	14606	
Physical quantity, property	Unit	Measurement ranges
Optical wavelength	nm	200..2500

Table 9-2 The Krypton line source

Equipment name / No	Krypton line source	***E8-48***
Manufacturer	LOT-Oriel	
Type	LSP031	
Serial No.	527909/004	
Physical quantity, property	Unit	Measurement ranges
Wavelength	nm	400..900

Table 9-3 The Ribbon filament lamp

Equipment name / No	Ribbon filament lamp	***S8-17***
Manufacturer	Tartu Observatory	
Type	SI300/10	
Serial No.	001	

Physical quantity, property	Unit	Measurement ranges
Spectral irradiance	W/mr/nm	0.001..1

Table 9-4 The Power supply

Equipment name / No	Power supply	***S8-13***
Manufacturer	L.O.T. Oriel	
Type	69935	
Serial No.	166	
Physical quantity, property	Unit	Measurement ranges
Voltage	V	0..150
Current	A	4..9

Table 9-5 The Shunt resistor

Equipment name / No	Shunt resistor	***S8-11***
Manufacturer	ZIP	
Type	P310	
Serial No.	009009	
Manufacturing date	1962	
Physical quantity, property	Unit	Measurement ranges
Electrical resistance	Ohm	0.01

Table 9-6 The Integrating sphere

Equipment name / No	Integrating sphere	***S8-33***
Manufacturer	Bentham Instruments Ltd	
Type	DIFF_D8_SLIT_FIBRE	
Serial No.	19155/1	
Physical quantity, property	Unit	Measurement ranges
Spectral radiance	W/m2/Sr/nm	N/A

Figure 9-1 The Bentham integrating sphere working principle.

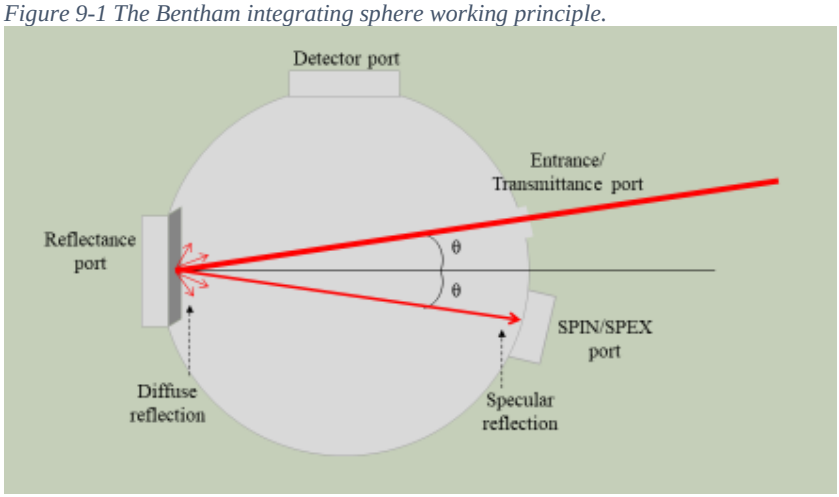

Table 9-7 The Alignment laser-LT52

Equipment name / No	Alignment laser	***S8-30***
Manufacturer	Spectra Precision	
Type	LT52	
Serial No.	002	
Physical quantity, property	Unit	Measurement ranges
Beam divergence	arc second	120

Table 9-8 The Alignment laser-XLC

Equipment name / No	Alignment laser	***S8-15***
Manufacturer	N/A	
Type	XCL	
Serial No.	001	
Physical quantity, property	Unit	Measurement ranges
Beam divergence	degree	0.02

Table 9-9 The Temperature controller

Equipment name / No	Temperature controller	***S8-19***
Manufacturer	Newport Corporation	
Type	350B	
Serial No.	110 206 016	

Physical quantity, property	Unit	Measurement ranges
Temperature	°C	10..40

Table 9-10 The Photomultiplier tube

Equipment name / No	Photomultiplier	***S8-31***
Manufacturer	Tartu Observatory	
Type	PMT-TO-1	
Serial No.	001	
Physical quantity, property	Unit	Measurement ranges
Electric current	A/lm	100 A/lm

Figure 9-2 The Photomultiplier tube

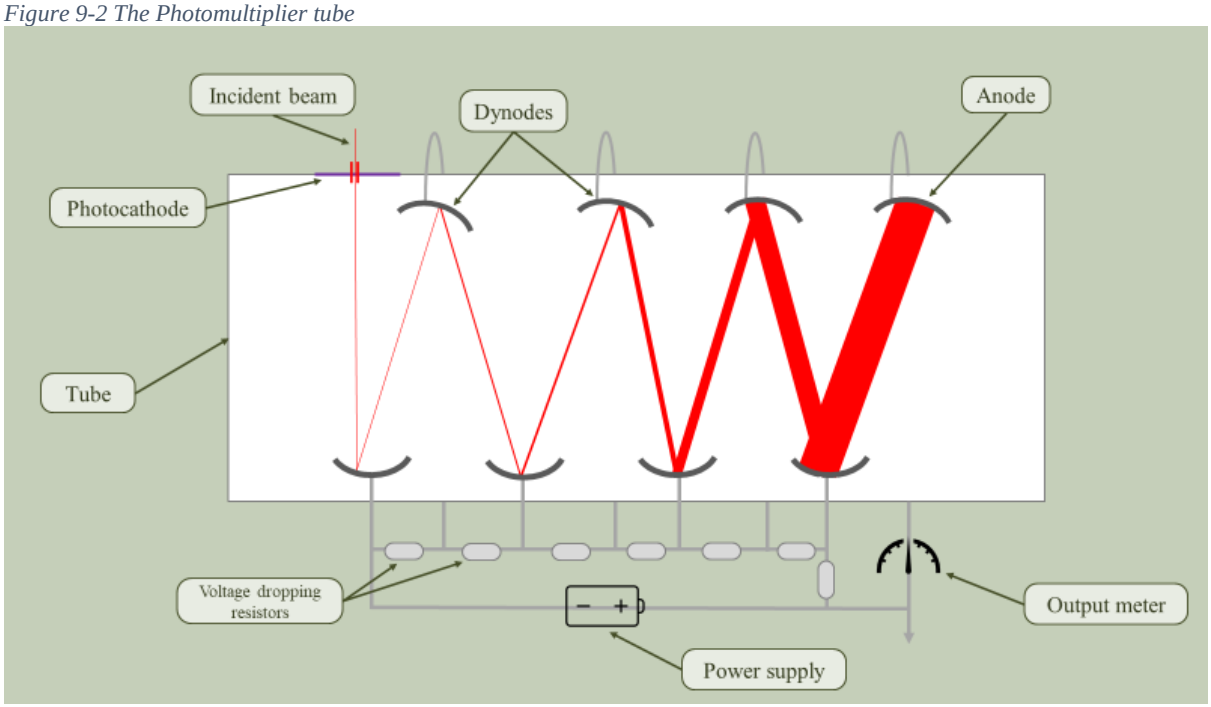

Table 9-11 The DC AMP/ADC

Equipment name / No	DC AMP/ADC	***E8-09***
Manufacturer	Bentham Instruments	
Type	487	
Serial No.	19717/2	
Physical quantity, property	Unit	Measurement ranges
Current	A	$10^{-11}..20*10^{-6}$

Figure 9-3 The DC AMP/ADC

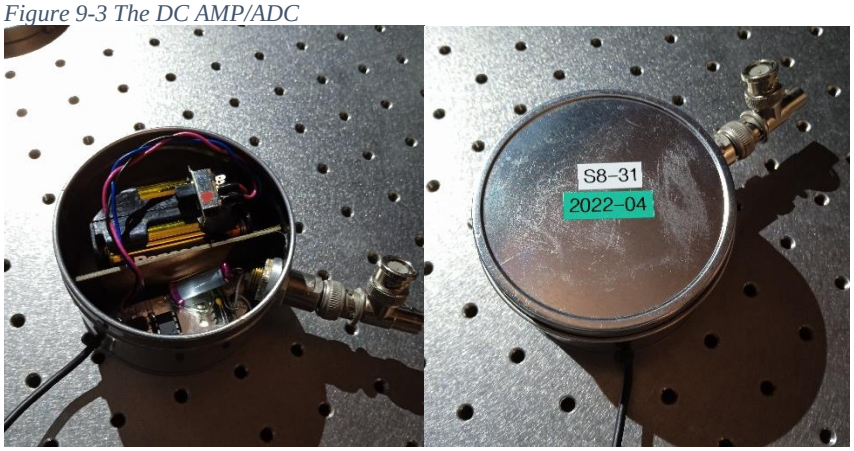

Table 9-12 The Filter radiometer

Equipment name / No	Filter radiometer	***S8-29***
Manufacturer	Hohenheide OÜ	
Type	HHFR03-S1337	
Serial No.	001	
Physical quantity, property	Unit	Measurement ranges
Spectral irradiance	$w/m^2/nm$	$10^{-6}..10^{-3}$

Figure 9-4 The schematic of the graph paper results.

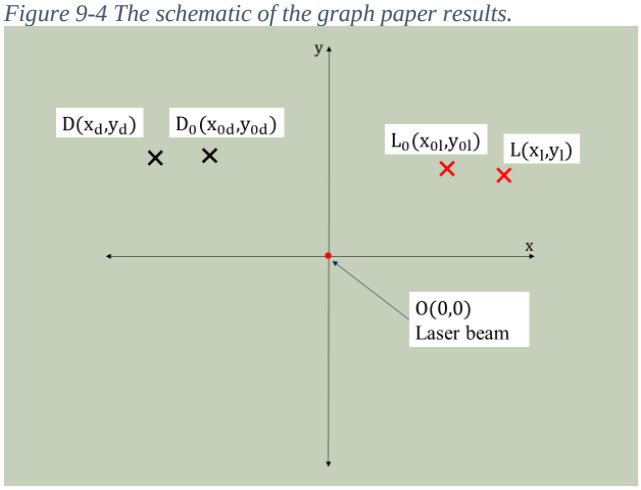

Table 9-13 Key parameters of WAS [20]

Parameter	WAS	Unit
weight*	1.2	kg
digital interface	USB	-
supply voltage	+5	V
power consumption	6	W
depth rating	N/A**	m
temperature range	0…+40	°C
field of view	3**	°
integration time	10…60000	ms
wavelength range	350…1000	nm
wavelength step	0.35	nm
wavelength accuracy	N/A	nm
spectral bandwidth	2***	nm
pixel count	2048	-
NER @ 500 nm	3.3	$\mu W m^{-2} nm^{-1} sr^{-1}$
radiance responsivity @ 500 nm & 1 ms	300	$\mu W^{-1} m^{2} nm sr$
minimum sampling interval	0.1	s
internal shutter	no**	-
thermal control	yes	-
internal temperature sensor	yes	-

*spectrometer only
**current prototype
***25 nm slit option

Figure 9-5 The Wasatch WP-VISNIR- R2-IC spectrometer module [20]

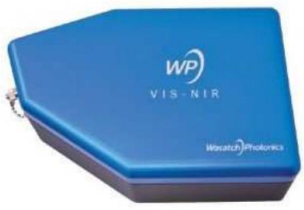

9.3. Tables

9.3.1. The Error% for the fitted spectra

Table 9-14 The Error% for some spectra fitted with various peak shapes, which Triangular shape best fits.

H mm \ Error%	Gaussian	Lorentzian	Voigt	Triangular	Flattened Gaussian	Rectangular
0	0.319	2.385	1.409	1.048	1.200	5.171
-2	13.101	2.383	1.407	1.085	1.209	5.167
-1	0.328	2.390	1.411	1.065	1.203	5.162
-0.5	0.324	2.379	1.403	1.048	1.214	5.170
0.5	0.322	2.373	1.400	1.050	1.205	5.164
1	12.880	2.356	1.389	1.045	1.207	5.154
2	12.981	2.356	1.392	1.090	1.185	5.169
0	0.318	2.386	1.409	1.050	1.202	5.169
0	0.321	2.373	1.399	1.055	1.207	5.171
average Error%	4.544	2.376	1.402	1.059	1.203	5.166

Table 9-15 The Error% for some spectra fitted with various peak shapes, which Gaussian shape best fits.

Hg	WL=	297 nm	500 V			
BW nm \ Error%	Gaussian	Lorentzian	Voigt	Triangular	Flattened Gaussian	Rectangular
0.05	3.331	18.284	18.090	3.585	15.244	16.476
0.20	1.703	24.570	24.159	2.350	1.287	20.661
0.50	1.567	31.849	30.488	2.720	2.609	15.366
1.00	2.432	7.754	5.532	2.513	1.728	17.927
2.00	2.835	9.283	6.587	3.191	2.248	14.621
3.00	2.866	9.264	6.531	3.085	2.082	14.473
average Error%	2.456	16.834	15.231	2.907	4.200	16.587

Table 9-16 The Error% for some spectra fitted with various peak shapes, which Flattened Gaussian shape best fits.

Hg	WL =	546 nm		BW=	1.00	nm
deviation mm \ Error%	Gaussian	Lorentzian	Voigt	Triangular	Flattened Gaussian	Rectangular
0	3.282	9.450	6.940	3.030	2.272	13.433
-2	3.005	8.219	5.838	3.067	2.492	14.565
-1	2.931	8.890	6.381	3.443	2.118	14.385
1	3.221	9.260	6.779	2.790	2.426	13.181
2	2.824	8.472	6.083	2.541	2.597	13.087
0	3.122	9.091	6.585	3.045	2.208	13.460
average Error%	3.064	8.897	6.435	2.986	2.352	13.685

Table 9-17 The Error% for some spectra fitted with various peak shapes, which none provide a good fit.

RFL	**Filter:**	**800 nm**		**BW=**	**1.00 nm**	
T °C \ Error%	Gaussian	Lorentzian	Voigt	Triangular	Flattened Gaussian	Rectangular
25	14.529	20.719	18.034	14.752	10.526	32.797
18	14.539	20.721	18.039	14.746	10.537	32.813
32	14.566	20.762	18.074	14.809	10.559	32.862
25	14.559	20.748	18.063	14.781	10.555	32.837
average Error%	14.548	20.738	18.053	14.772	10.544	32.827

9.3.2. The alignment table

setup	Distance	Angle	Line	Delta CWL
alignment #1	8.65 mm	1.42°	Hg 0'th order	0.0010 nm
			Hg 296,6 nm	0.0018 nm
			Kr 877 nm	0.0015 nm
			RFL 55 nm	0.0022 nm
alignment #2	0 mm	0°	Hg 0'th order	0.0015 nm
			Hg 296,6 nm	0.0021 nm
			Kr 877 nm	0.0015 nm
			RFL 55 nm	0.0012 nm
alignment #3	0.89 mm	0.15°	Hg 0'th order	0.0015 nm
			Hg 296,6 nm	0.0017 nm
			Kr 877 nm	0.0023 nm
			RFL 55 nm	0.0005 nm
alignment #4	7.79 mm	1.28°	Hg 0'th order	0.0034 nm
			Hg 296,6 nm	0.0018 nm
			Kr 877 nm	0.0026 nm
			RFL 55 nm	0.0016 nm
Integrating sphere	N/A	N/A	Hg 0'th order	0.0021 nm
			Hg 296,6 nm	0.0011 nm
			Kr 877 nm	0.0030 nm
			RFL 55 nm	0.0024 nm

9.4. Figures

Figure 9-6 The main software window

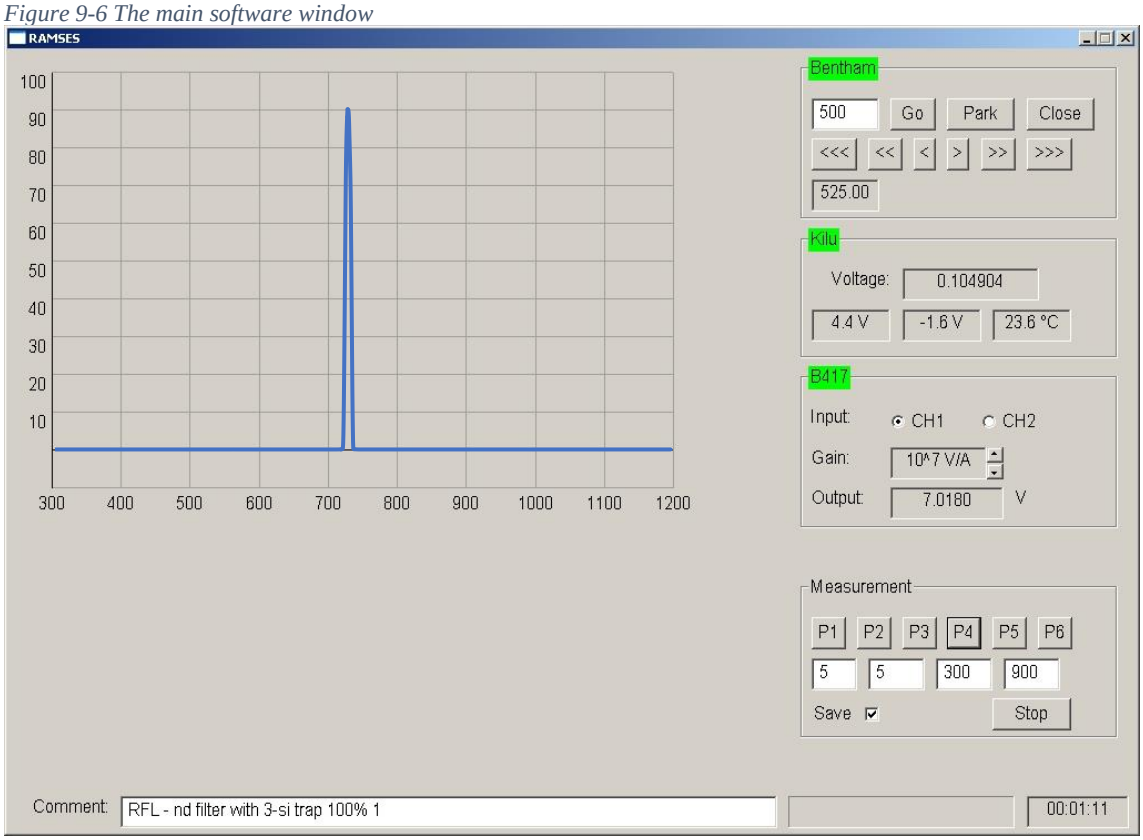

Figure 9-7 The schematic of the #2 and #4 alignment setup, incident beam, reflected beam, α_2, and β_2.

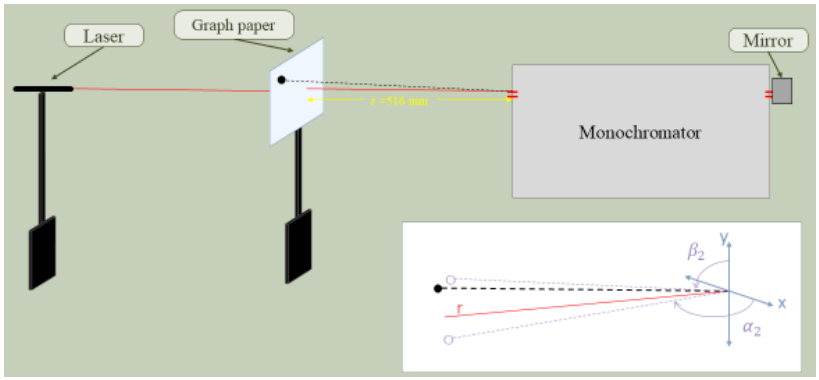

Figure 9-8 The results of transmittance measurements for the Neutral density filter.

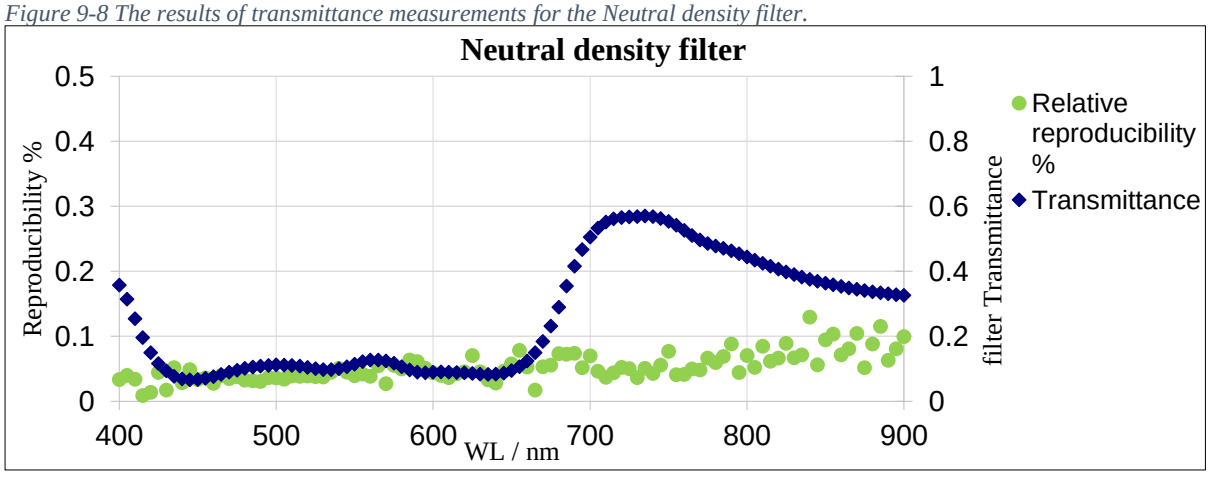

9.5. Convolution technique

The convolution technique is performed by applying the following steps:

- Define the stray light kernel: The stray light kernel represents the spectral response of the stray light present in the system. This can be obtained through experimental measurements or by modeling the optical system. The kernel describes how the stray light affects the measured signal as a function of wavelength.
- Obtain the measured spectral data: This refers to the raw spectral data obtained from the experimental setup or instrument. It represents the observed signal, which includes the contributions from both the desired signal and the stray light.
- Perform convolution: The measured spectral data is convolved with the stray light kernel. This mathematical operation involves multiplying the spectral data at each wavelength point with the corresponding value from the stray light kernel and summing up the results. The convolution operation effectively integrates the stray light contribution over the entire spectrum.
- Assess the bias caused by stray light: The result of the convolution operation represents the estimated stray light contribution to the measured signal. The bias caused by uncorrected stray light can be assessed by comparing the convolved data with the measured data. This allows for quantitative analysis of the stray light impact on the filter transmittance.
- Correct for stray light bias: The convolution technique provides valuable information about the stray light bias. Based on this information, appropriate correction methods can be applied to account for the stray light contribution and obtain a more accurate measurement of the filter transmittance. These correction methods may involve subtracting the convolved stray light component from the measured data or applying calibration factors.

By utilizing the convolution technique, the bias caused by uncorrected stray light can be quantified, evaluated, and corrected, leading to improved accuracy and reliability of the filter transmittance measurement.

UNCERTAINTY OF THE OPTICAL SPECTRAL TRANSMITTANCE

Abstract: Determination of the optical filter spectral transmittance takes place at Tartu Observatory and is one of the accredited methods of the Tartu University Testing Centre. Comprehensive characterization of the measurement setup forms the experimental part of this master thesis. The measurement principles, instrumentation, and techniques are described in detail. In conclusion, the uncertainty contributions were quantified, and recommendations were given in order to improve the measurement setup. The thesis can be used as step-by-step instructions when reproducing the characterization of similar systems.

Keywords: optical transmittance, characterization, uncertainty

CERCS code: P180

OPTILISE SPEKTRAALSE LÄBILASKVUSE MÕÕTEMÄÄRAMATUS

Kokkuvõte: Optiliste filtrite spektraalse läbilaskvuse mõõtmine Tartu Observatooriumi optikalaboris kuulub Tartu Ülikooli Katsekoja akrediteeritud meetodite hulka. Magistritöö käigus viidi läbi mõõtesüsteemi põhjalik karakteriseerimine. Detailselt on kirjeldatud mõõtmise aluspõhimõtted, aparatuur ja mõõtemeetodid. Töö tulemusena täpsustati määramatuse komponente ja anti soovitused meetodi täiustamiseks. Magistritöö on kasutatav käsiraamatuna sarnaste süsteemide karakteriseeriminsel.

Märksõnad: optiline läbilaskvus, karakteriseerimine, mõõtemääramatus

CERCS kood: P180

Non-exclusive licence to reproduce the thesis and make the thesis public

I, **Zeinab Chehreghan**,

1. grant the University of Tartu a free permit (non-exclusive licence) to

reproduce, for the purpose of preservation, including for adding to the DSpace digital archives until the expiry of the term of copyright, my thesis

UNCERTAINTY OF THE OPTICAL SPECTRAL TRANSMITTANCE,

supervised by **Ilmar Ansko**,

2. I grant the University of Tartu a permit to make the thesis specified in point 1 available to the public via the web environment of the University of Tartu, including via the DSpace digital archives, under the Creative Commons licence CC BY NC ND 4.0, which allows, by giving appropriate credit to the author, to reproduce, distribute the work and communicate it to the public, and prohibits the creation of derivative works and any commercial use of the work until the expiry of the term of copyright.

3. I am aware of the fact that the author retains the rights specified in points 1 and 2.

4. I confirm that granting the non-exclusive licence does not infringe other persons' intellectual property rights or rights arising from the personal data protection legislation.

Zeinab Chehreghan

23/05/2023